B55α/PP2A Limits Endothelial Cell Apoptosis During Vascular Remodeling: A Complementary Approach To Kill Pathological Vessels?

Manuel Ehling[1,2], Ward Celus[1,2], Rosa Martín-Pérez[1,2], Roser Alba-Rovira[1,2,3], Sander Willox[1,2], Donatella Ponti[1,2,4], Maria C. Cid[3], Elizabeth A. V. Jones[5], Giusy Di Conza[1,2], Massimiliano Mazzone[1,2]

[1]Laboratory of Tumor Inflammation and Angiogenesis, Center for Cancer Biology (CCB), VIB, Leuven, 3000; [2]Laboratory of Tumor Inflammation and Angiogenesis, Oncology, KU Leuven, Leuven, 3000; [3]Vasculitis Research Unit, Department of Autoimmune Diseases, Hospital Clínic, University of Barcelona, Institut d'Investigacions Biomèdiques August Pi I Sunyer (IDIBAPS), Barcelona; [4]Medical-Surgical Sciences and Biotechnologies, University of Rome Sapienza, Corso della Repubblica 79, 04100, Latina; [5]Cardiovascular Sciences, KU Leuven, 3000 Leuven.

***Running title*:** B55α in Vascular Biology

Subject Terms:
Angiogenesis
Cell Signaling/Signal Transduction
Developmental Biology
Mechanisms
Vascular Biology

Address correspondence to:
Dr. Massimiliano Mazzone
Laboratory of Tumor Inflammation and Angiogenesis
Center for Cancer Biology (CCB)
VIB, Leuven, 3000
massimiliano.mazzone@kuleuven.vib.be

ABSTRACT

Rationale: How endothelial cells (ECs) migrate and form an immature vascular plexus has been extensively studied. Yet, mechanisms underlying vascular remodeling remain poorly established. A better understanding of these processes may lead to the design of novel therapeutic strategies complementary to current angiogenesis inhibitors.

Objective: Starting from our previous observations that the PP2A phosphatase regulates the HIF/PHD2-constituted oxygen machinery, we hypothesized that this axis could play an important role during blood vessel formation, tissue perfusion and oxygen restoration.

Methods and Results: We show that the regulatory PP2A-phosphatase subunit B55α is at the crossroad between vessel pruning and vessel maturation. Blood vessels with high B55α will counter cell stress conditions and thrive for stabilization and maturation. When B55α is inhibited, ECs cannot cope with cell stress and undergo apoptosis, leading to massive pruning of nascent blood vessels. Mechanistically, we found that the B55α/PP2A complex restrains PHD2 activity, promoting EC survival in a HIF-dependent manner, and furthermore dephosphorylates p38, altogether protecting ECs against cell stress occurring, for example, during the onset of blood flow. In tumors, EC-specific B55α deficiency induces pruning of immature-like tumor blood vessels resulting in delayed tumor growth and metastasis, without affecting non-pathological vessels. Consistently, systemic administration of a pan-PP2A inhibitor disrupts vascular network formation and tumor progression *in vivo* without additional effects on B55α-deficient vessels.

Conclusions: Our data underline a unique role of the B55α/PP2A phosphatase complex in vessel remodeling and suggest the use of PP2A-inhibitors as potent anti-angiogenic drugs targeting specifically nascent blood vessels with a mode-of-action complementary to VEGF(R)-targeted therapies.

Keywords:
Angiogenesis, B55α/PP2A-phosphatase, development, tumor progression, apoptosis, transgenic model, tumor, apoptosis.

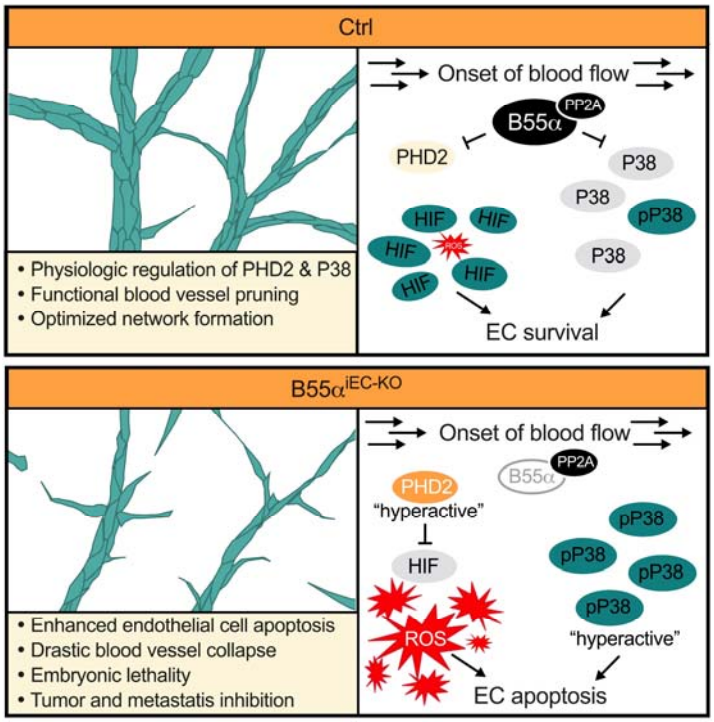

Nonstandard Abbreviations and Acronyms:

AKT1	AKT Serine/Threonine Kinase 1
AMPK	AMP-activated protein kinase
ATF4	activating transcription factor 4
CD31	cluster of differentiation 31
cl.Casp3	cleaved Caspase 3
ColIV	Collagen IV
DMOG	dimethyloxalylglycine
EC	endothelial cell
EdU	5-ethynyl-2'-deoxyuridine
eIF2α	eukaryotic initiation factor 2 alpha
ERK	extracellular signal-regulated kinases
FOXO1	forkhead box protein O1
NT	non treated
HIF	hypoxia-inducible factor
HMVECs	human microvascular ECs
HUVECs	human umbilical vein endothelial cells
IsoB4	isolectin griffonia simplicifolia B4
JNK	c-Jun N-terminal kinases
KD	knockdown
KO	knockout
LEC	lymphatic endothelial cell
LLC	lewis lung carcinoma
MnTBAP	Mn(III)tetrakis(4-benzoic acid)porphyrin chloride
Nec1	necrostatin-1
NFkB	nuclear factor kappa-light-chain-enhancer of activated B cells
NRF2	nuclear factor erythroid 2-related factor 2
OE	overexpression
o/n	over night
PHD	hypoxia-inducible factor prolyl hydroxylase 2
PKR	protein kinase R
PP2A	protein phosphatase 2
qVD	5-(2,6-Difluorophenoxy)-3-[[3-methyl-1-oxo-2-[(2-quinolinylcarbonyl) amino]butyl]amino] -4-oxo-pentanoic acid hydrate
ROS	reactive oxygen species
VEGF-R	vascular endothelial growth factor receptor
zIETDS	L-Threoninamide, N-[(phenylmethoxy)carbonyl]-L-isoleucyl-L-α-glutamyl-N-[(1S)-3-fluoro-1-(2-methoxy-2-oxoethyl)-2-oxopropyl]-, methyl ester
zVAD	z-Val-Ala-DL-Asp(OMe)-fluoromethylketone

INTRODUCTION

The formation of the first vascular network is characterized by fusion of tip cells and the subsequent start of blood vessel perfusion[1]. However, this immature plexus is still inefficient and lacks a clear distinction between arteries, capillaries and venous structures[2, 3].

To create a mature network, this plexus undergoes several remodeling processes, including the removal of supernumerary capillaries. The latter is mediated either by coordinated cell migration or

induction of apoptosis[4-6], which have to be tightly regulated to avoid an inadequate blood flow supply to organs[7].

In contrast to sprouting angiogenesis, mechanisms controlling vascular remodeling and apoptosis-mediated blood vessel pruning remain less clear, especially in regard to blood flow induced cell stress[8-11]. As one example, HIF-signaling protects ECs against ROS arising upon vessel perfusion[9, 12-14]. Moreover, also the p38 pathway mediates a tightly balanced cell stress response. While short term activation of p38 promotes cell survival and differentiation, prolonged p38 activation induces apoptosis in ECs[15].

A better understanding of how these remodeling processes are regulated, could reveal novel therapeutic intervention points for clinical applications. Given the pivotal role of VEGF signaling in vessel sprouting[16] and maintenance[17], most currently used angiogenesis inhibitors target VEGF or its receptors[18]. However, these drugs only prolong the survival of cancer patients without cure and often display severe side effects[19, 20]. Novel agents, with alternative mechanisms of action, could overcome the limits of VEGF-targeted therapies.

Here, we analyzed the role of the PP2A phosphatase subunit B55α during vascular development and cancer progression. B55α is one of 26 regulatory subunits which orchestrate the activity and substrate specificity of the trimeric PP2A phosphatase complex[21]. Inhibition of B55α in cancer cells alleviates tumor progression by reducing cell viability in hypoxia and glucose starvation[22, 23]. However, besides one publication in zebrafish[24], the role of B55α in stromal cells remains unknown. Here, we found that genetic deletion of B55α unleashes apoptosis-mediated blood vessel pruning during development and cancer progression. In two different tumor models, we show that genetic loss of B55α in ECs or pharmacologic inhibition of the PP2A phosphatase has a strong anti-angiogenic effect specifically targeting immature tumor vessels, thereby delaying tumor and metastatic progression.

METHODS

A detailed Methods section can be found in the Online Data Supplement. Major Resources Table in the Supplemental Materials contain the list of all the main reagents used.

The authors declare that the majority of supporting data are presented within this article and its Online Data Supplement. Data that are not directly available are available from the corresponding author upon reasonable request.

All sequencing data are deposited in the ArrayExpress database under accession code E-MTAB-9002.

RESULTS

B55α controls EC survival during developmental vascular remodeling.

Our initial analysis revealed a conservation rate of 100% between human and murine B55α protein (Fig. 1A), pointing to a very unique role of this regulatory subunit.

We then analyzed the expression pattern of *Ppp2r2a* (the gene coding for B55α) using RNAscope. In mouse embryos, RNA expression of B55α was detectable in several cell types including $CD31^+$ blood

vessels (Fig. 1B). In adult mice, expression of B55αwas strongly diminished if not absent, while markedly detectable in sites of active angiogenesis such as progressing tumors (Online Fig. I A-E). We therefore hypothesized that B55α might be required in the immature vascular plexus while being dispensable in the quiescent vasculature of adults (see text further below and Online Fig. IV).

To analyze the functional role of B55α, we generated embryos with homo- and heterozygous deletion for the *Ppp2r2a* gene (Online Fig. I G). Deletion efficiency was confirmed at embryonic stage E12.5 on RNA and protein levels (Fig. 1C-E). In line with the high conservation rate, *Ppp2r2a* gene deletion led to embryonic lethality around E14.5 not only in homozygous, but also in 60% of heterozygous knockout (KO) embryos (Fig. 1F). However, surviving heterozygous mice reached the adult stage, were fertile and did not show any obvious defects at steady conditions.

In contrast, homozygous KO embryos displayed severe bleedings in their skin (Fig. 1G), suggesting that these mutants suffered from vascular defects. Analysis of skin samples at E14.5 allowed us to differentiate between vascular defects in areas of initial vascularization and blood vessel remodeling (Online Fig. I K-N).

Although remodeling blood vessels were strongly affected (Fig. 1H-K), we did not observe any changes in the initially formed immature vascular plexus (Online Fig. II A,B). In addition, mutant embryos displayed aberrant lymphatic vessel structures (Fig. 1L,M), which appeared less organized and even completely disrupted in homozygous KO mice.

To analyze the selective role of B55α in ECs, *Ppp2r2a(lox/lox)* conditional KO mice were intercrossed with the tamoxifen-inducible VE-cadherin.CreERT2 deleter strain (henceforward B55$^{iEC\text{-}KO}$) (Online Fig. I G,I). In line with the results in Full-KO embryos, genetic deletion of B55 in ECs led to bleedings in the skin of mutant B55α$^{iEC\text{-}KO}$ embryos (Fig. 2A) accompanied by vascular and lymphatic defects in regions of vascular remodeling (Fig. 2B-F).

In contrast, there was no obvious phenotype during the initial steps of blood vessel formation neither in embryonic skin nor in postnatal retina samples (Online Fig. II C-J). B55α deletion drastically increased the frequency of apoptotic ECs in mutant embryos (Fig. 2G,I) and retina samples (Online Fig. II K-O) where the majority of apoptotic events occurred in luminized (Icam2^{+}) blood vessels[25] and thus before the collapse of these vessels (Online Fig. II P). This is in line with our results in the embryonic skin, showing that the induction of apoptosis preceded the morphological changes in more mature areas of the same vascular plexus (Online Fig. II E,F). Altogether, our data suggest that EC apoptosis in mutants precedes and might even cause the drastically enhanced blood vessel pruning in the remodeling plexi (Fig. 2H,J). As a final result of the progressing vascular defects, EC-specific deletion of B55αled to embryonic lethality by E16.5 (Fig. 2K-O).

Similar to the defects in full KO embryos (Fig. 1L,M), pan-endothelial deletion of B55αresulted in enlarged and activated lymph vessels in embryonic skin samples (Fig. 2C,E,N,O). However, B55αdeletion specifically in lymphatic ECs (using Prox1.CreERT2 mice) did not recapitulate these defects (Online Fig. III A-F), indicating that the lymphatic phenotype in B55α$^{iEC\text{-}KO}$ mice might be secondary to the strong vascular defects.

Lack of endothelial B55αdelays tumor progression.

In contrast to the developmental phenotype, inducible EC-specific (B55α$^{iEC\text{-}KO}$) or ubiquitous (B55α$^{iR26\text{-}KO}$) deletion of B55a in 8-10 weeks old mice did not lead to lethality or any overt organ defects (Online Fig. IV A-U). Equally treated mice reached an age beyond 50 weeks without displaying any

pathological signs (Online Fig. IV A,C). The histological analysis of different organs from adult B55α^{iEC-KO} mice did not reveal any vascular or lymphatic defect (Online Fig. IV F-U). This is consistent with the downregulated *Ppp2r2a* expression in quiescent blood vessels of adult mice (Online Fig. I A-C) and indicates that B55αis dispensable for the maintenance of vessel quiescence.

Since tumor blood vessels are mainly immature[26] and express high levels of *Ppp2r2a* (Online Fig. I D,E), we wondered whether B55αinhibition would also induce pruning of these vessels. We thus injected either LLC cells subcutaneously or E0771 breast cancer cells orthotopically in tamoxifen-treated control and B55α^{iEC-KO} mice. We observed that EC-specific deletion of B55αresulted in a strongly delayed tumor progression and metastasis formation in both models (Fig. 3A-F), which was also recapitulated by ubiquitous deletion of B55α (Online Fig. IV X). The decrease in tumor size and weight (Fig. 3B,E) was accompanied by enhanced tumor hypoxia and necrosis (Fig. 3G-N), while cancer cell extravasation and lodging to the lung was not altered by lack of B55α (Online Fig. IV Y).

Analysis of blood vessels in progressing tumors of B55α^{iEC-KO} mutant mice revealed that these had an altered shape, were less dense and less well connected when compared to controls (Fig. 3O-S,V). Reminiscent to the developmental phenotype, lack of B55αled to an increased number of apoptotic ECs within the tumor vasculature (Fig. 3S-U,V-X). At the same time, the retinal vasculature of tumor-bearing mice appeared normal and showed no significant differences between the two genotypes (Online Fig. IV V,W).

B55α deletion after tumor resection inhibits metastatic growth and prolongs survival.

Our results in cancer cells[22, 23] and the current data in ECs suggest that pharmacologic inhibition of B55α/PP2A might represent an interesting approach in cancer therapy. However, many patients relapse at a distant site long after the primary tumor has been surgically resected. Thus, approaches inhibiting metastasis progression, accounting for the majority of cancer-related deaths[27], are currently needed.

To mimic this clinical setting, we injected wildtype LLC cancer cells in mice not yet treated with tamoxifen (Fig. 4A). In line with the non-recombined *Ppp2r2a* gene, tumors in these mice progressed identical (Fig. 4B). Tumors were then surgically removed and after 3 days of recovery tamoxifen treatment was initiated in order to induce EC-specific *Ppp2r2a* deletion. As compared to control mice, EC-specific *Ppp2r2a* deletion conferred longer survival and a drastic reduction in lung metastasis (Fig. 4C-H). Albeit having similar numbers of lung metastasis (Fig. 4D), lack of endothelial B55α led to a delayed progression of these metastatic lesions (Fig. 4E-H). Similar to the effects observed in primary tumors, blood vessel density within the angiogenic active metastatic site was strongly impaired (Fig. 4I-J).

Pharmacologic PP2A inhibition induces vessel pruning and delays tumor progression.

Although specific inhibitors for the B55αPP2A are not currently available yet, the pan-PP2A inhibitor LB100, which blocks the catalytic PP2A subunit, was recently approved in a clinical phase I study for use in patients with 2 additional phase II clinical trials still ongoing[28-30].

In order to test whether LB100-mediated pharmacologic inhibition of PP2A had an anti-angiogenic effect, without affecting cancer or stromal cells directly, we implanted sponges conditioned with tumor-conditioned medium to monitor angiogenesis (Fig. 5A)[31]. Even at low doses, LB100 treatment disrupted the immature vascular network formation in sponges of wildtype mice but had no additional effects in B55α^{iEC-KO} mice (Fig. 5B,C).

We then analyzed the effects of low dose LB100 treatment on tumor progression and found that LLC tumor growth was reduced to a similar extent as in B55^{iEC-KO} (Fig. 5D,E) without showing any overt signs of toxicity (Fig. 5F). The reduced blood vessel density was comparable in B55α^{iEC-KO} and LB100-treated mice (Fig. 5G,H) and resulted in increased tumor hypoxia under both conditions (Fig. 5I,J). As observed in B55α^{iEC-KO} tumor-bearing mice, inhibition of PP2A by LB100 did not alter the ratio of pericyte-covered tumor blood vessels, suggesting that only vessel numbers, but not blood vessel maturation *per se* was affected (Online Fig. IV Z).

B55αdeficiency induces apoptosis in maturating ECs but not in other cell types.

We then used either sparse or densely seeded HUVECs to study the role of B55α in EC apoptosis *in vitro*. As shown by others[32, 33] and by us (Online Fig. V A,B), this is a simplified system comparing proliferative *versus* contact-inhibited (non-proliferative) ECs.

Compared to sparse ECs, B55α was strongly upregulated in densely-seeded ECs at both mRNA and protein levels (Fig. 6A,B). In contrast, B55b was barely detectable in HUVECs, while B55c showed the highest expression in sparse ECs and, similar to B55, αB55d was upregulated in dense HUVECs (Online Fig. V C-E). However, only KD of B55α, but not of any other B55-subunit, led to an apoptosis-mediated decrease of densely seeded HUVECs (Fig. 6C-F, Online Fig. V F-N). Furthermore, only treatment with the pan-Caspase inhibitors zVAD or qVD (Fig. 6G-I), but not the inhibition of necroptosis or extrinsic apoptosis (via block of Caspase8) counteracted cell death in B55α-KD HUVECs (Online Fig. V O,P), suggesting that loss of B55α activates the intrinsic apoptotic pathway in ECs.

This effect was phenocopied by treatment with the pan-PP2A-inhibitor LB100 but far less pronounced in sparse HUVECs (Fig. 6E, J-M). PP2A inhibition in different cancer cell lines, macrophages or LECs did not induce apoptosis (Online Fig. V Q,R; Online Fig. III G-K).

Altogether, our *in vivo* and *in vitro* data suggest that B55α/PP2A promotes an anti-apoptotic program which is relevant for the survival of vascular ECs in neoformed vessels but not of sprouting ECs, LECs or other cell types.

B55α counteracts ROS in a PHD/HIF dependent manner.

Expression of B55α in densely cultured ECs was further increased by flow conditions (Online Fig. V S,T). Moreover, the presence of the ROS-scavenging molecule MnTBAP[34, 35] during growth of HUVECs from sparse to dense conditions, strongly prevented B55α upregulation (Fig. 7A). We thus hypothesized that B55α might counteract ROS in newly perfused vessels. Given the involvement of PHD2/HIF in vessel remodeling[22, 36] and ROS scavenging[9, 12-14], as well as our previous work showing a B55α–mediated regulation of PHD2 activity and vice versa[22, 23], we initially focused on this signaling axis.

We found that densely-seeded HUVECs were indeed protected against H_2O_2 induced ROS-stress in a B55α-dependent manner (Fig. 7B,C; Online Fig. VI A). In line with our work in cancer cells, protein levels of HIF1α and HIF2α were strongly reduced upon B55α–KD (Fig. 7D), arguing that B55α accumulation in dense HUVECs stabilized HIF1α and HIF2α proteins under normoxia. In contrast, there was a slight increase at the mRNA level upon KD of B55a (Online Fig. VI B-G), which might be an attempt of the cell to counteract the decreased HIF-protein levels. In line with our previous data in cancer cells, this suggests that the reduced stability of HIF proteins was mediated by increased PHD activity in B55a-KD HUVECs[22].

Functionally, overexpression (OE) of HIF1α or HIF2α counteracted the induction of apoptosis in B55a-KD HUVECs (Online Fig. VI H,I). Furthermore, also the pan-PHD inhibitor DMOG reduced cell stress in B55α–KD HUVECs, indicated by decrease in phospho-eIF2αand p21 and decreased apoptosis induction, indicated by cleaved Caspase3 (Fig. 7E). At the same time, phosphorylation levels of p38 were not normalized upon DMOG treatment (Fig. 7F), suggesting that this pathway might be regulated independent of the PHD/HIF signaling axis.

Exposure of sparse HUVECs to low doses of H_2O_2 led to an upregulation of B55α while not affecting ROS-protected, dense ECs (Fig. 7G). In contrast, exposure to high doses of H_2O_2, (500μM), which was lethal for sparse HUVECs, increased B55α expression in dense HUVECs. This supports the idea that ECs upregulate B55α in order to counteract otherwise lethal levels of ROS. In line, DMOG treatment in B55α–KD HUVECs (Fig. 7H) restored the expression of ROS-scavenging genes (Fig. 7I; Online Fig. VI J-M). As a consequence, DMOG-treated B55α-KD HUVECs showed a restored capacity to counteract ROS and a partial but significant rescue in cell survival (Fig. 7J-L).

To show the direct effect of this signaling axis on ECs *in vivo* (without involvement of stroma or cancer cells), we performed sponge assays in control and $B55\alpha^{iEC\text{-}KO}$ mice. In line with our *in vitro* results, sponges implanted in $B55\alpha^{iEC\text{-}KO}$ mice had very few blood vessels and DMOG treatment led to a significant rescue (Fig. 7M,N).

Though DMOG is a pan-PHD inhibitor, based on our previous findings[22, 23] we can speculate that B55α is upregulated in ECs in order to elicit a HIF-mediated anti-oxidative program via PHD2 inhibition[22] thereby protecting the nascent endothelium against oxidative stress that may occur at the onset of blood flow[9, 12-14].

B55α/PP2A modulates a cell stress response by dephosphorylating p38.

Given that block of PHD only partially rescued survival of ECs lacking B55α, we analyzed the regulation of other signaling pathways involved in cell stress responses, such as NFκB, NRF2, Foxo1 and ATF4. However, we could not detect any change (Online Fig. VI N-Q).

We therefore performed RNAseq on dense control and B55α–KD HUVECs treated with the pan-Caspase inhibitor qVD, avoiding artefacts resulting from apoptosis induction. In line with the above results, KD of B55α led to a strongly diminished response to oxidative stress (Online Fig. VII A). In addition, we found a strong increase in p38 signaling as well as other cell stress pathways such as NRF2, ATF signaling upon KD of B55α. We decided to focus on the p38 pathway since *(i)* many of these pathways are regulated in a p38-dependent manner[22, 37-39], *(ii)* nuclear localization of the main executors of the other pathways did not change (Online Fig. VI N-Q), (*iii)* PP2A has been previously reported to dephosphorylate p38[15, 40]. We found that KD of B55α strongly increased p38 phosphorylation (Fig. 8A), an effect persistent after inhibition of PHD2 (Fig. 7F). In contrast, there were no changes in activation or total protein levels of other stress sensors such as ERK or JNK (Online Fig. VI R,S).

We thus hypothesized that B55α/PP2A might be able to regulate p38α signaling either directly or indirectly by modulating upstream activators such as AMPK and PKR[15, 41, 42]. By performing co-immunoprecipitation experiments we found a direct binding of B55α to p38 (Fig. 8B, Online Fig. VI T,U), but not with AMPK, PKR or other cell stress kinases such as JNK and ERK (Online Fig. VI V,W,X).

Prolonged phosphorylation and hyper-activation of p38 induces apoptosis in ECs[15]. Consistently, chemical inhibition of p38 improved survival in B55α-KD ECs by normalizing p38 activity levels in these

cells (Fig. 8C-E). In control ECs p38 inhibition promoted cell death as well, by generating too low levels of p38 activation (Fig. 8C-E)[15].

Using the sponge implantation model, we found that chemical inhibition of p38 led to a dose-dependent improvement of blood vessel density in B55α^{iEC-KO} mice while having the opposite effect in control mice (Fig. 8F-H). This supported the idea that p38 activity, tightly controlled by the B55□/PP2A phosphatase, is relevant for the optimal formation of blood vessels.

DISCUSSION

To generate a highly effective and functional vascular network, a plethora of well-coordinated and tightly regulated remodeling processes occur at the same time. In contrast to early steps of angiogenesis, these later maturation processes are only poorly understood.

Here, we found that B55α plays an important role specifically in the remodeling vasculature. Consistently, genetic deletion of B55α led to enhanced EC apoptosis within the remodeling plexus and drastically increased pruning of immature blood vessels. However, chemical pan-PP2A inhibition had no additional effect on blood vessel pruning in B55α^{iEC-KO} mice, suggesting that vascular remodeling is mainly regulated by the B55α/PP2A holocomplex but none of the other 26 regulatory subunits.

Although we also observed strong lymphatic defects following pan-endothelial B55α deletion, selective deletion in lymphatic ECs only, did not recapitulate these defects. This suggests that the lymphatic phenotype in B55α^{iEC-KO} mice is secondary to the strong vascular defects. The subsequent increase of hypoxic areas could either affect LECs either directly or via lymphatic growth factors secreted by activated perivascular stromal cells[43-45]. Alternatively, a reduced vascular density may increase capillary pressure and cause chronic edema, augmenting intralymphatic pressure and lymphatic vessel dilatation[46].

Vascular B55α expression is important when some of the newly formed vessels are stabilized while others are pruned away, overall increasing the efficiency of tissue perfusion. The expression of B55α allows immature blood vessels to undergo maturation while ECs lacking B55α would be unprotected against cell stress induced by blood flow or the harsh tumor microenvironment. As a result, deletion of B55α decreased the density of the vascular network by inducing EC apoptosis and hyperpruning of nascent blood vessels. However, lack of B55α did not affect angiogenic sprouting or ECs in fully mature blood vessels.

Upregulation of B55α in ECs was recently linked to activated integrin α5β1[47]. In addition, our data show that not only cell density, accompanied by stabilized junctions, but also flow increased B55α expression. It is therefore tempting to speculate whether the mechanosensory complex might play a role in the upregulation of B55α in these contexts.

The role of B55α in vessel stabilization is supported by another publication performed in zebrafish embryos[24]. Mechanistically, this previous study suggested that EC apoptosis might be secondary to reduced blood flow after blood vessel collapse[48]. In contrast, the combination of our *in vitro* and *in vivo* data show that EC apoptosis in B55α-deficient remodeling blood vessels precedes the collapse and retraction of immature blood vessels. The lack of sprouting defects and identical vessel densities in the immature vascular plexus also suggest that ECs did not just become less responsive to angiogenic stimuli *per se*.

Since the onset of blood flow leads to a burst of ROS, ECs in newly perfused vessels have to counteract this sudden cell stress. Our previous work showed an interaction between B55α and PHD2/HIF,

with the latter being involved in ROS-mediated cell stress scavenging[9, 10, 12-14]. In the current work, we found that B55α engaged vasoprotective HIF[12, 49] which induced expression of genes counteracting ROS. We show that the downmodulation of these HIF-mediated pathways following B55□/PP2A knockdown occurs in a condition of dense, but normoxic EC cultures. However, in our previous work inhibition of B55α/PP2A phosphatase led to cancer cell apoptosis in response to oxygen or glucose restriction[22, 23]. Our current model in ECs suggests that B55α is upregulated and plays a role in the remodeling of the primitive vascular network during the initial onset of blood flow. Therefore, it is possible that under *in vivo* conditions, limited oxygen and nutrient availability, characterizing the tumor microenvironment, could exacerbate the pro-apoptotic signaling observed in B55α-KD ECs even more.

PHD inhibition only partially rescued improved survival of B55α-KD ECs *in vitro* and *in vivo*, thus implying the involvement of PHD-independent mechanisms. In this context, a proper balance of p38 activation (a known interactor of PP2A) is crucial for EC survival under cell stress conditions[15]. While the initial activation of p38 can be triggered by multiple stimuli such as cell stress or growth factors[50], complete loss of p38 as well as overactivation leads to vascular malformations and induction of EC apoptosis[15, 51, 52]. Here we show that B55α/PP2A maintains this fine balance of p38 activation by dephosphorylating and thus normalizing p38 signaling.

Our *in vitro* RNAseq data showed that a plethora of genes were changed upon KD of B55α in HUVECs. Although many of these changes can be explained by modulation of p38 and PHD2, we are not excluding that B55α/PP2A could dephosphorylate additional substrates[47]. In the context of blood vessel remodeling however, our rescue experiments performed *in vitro* and *in vivo* strongly support the idea that p38 and PHD2 are at least highly important, if not the main targets of B55α.

From a therapeutic point-of-view, we show that both genetic deletion of B55α and PP2A inhibition hinder tumor growth by inducing EC apoptosis in immature blood vessels. Furthermore, genetic deletion of B55α reduced the metastatic burden and extended survival in a model of metastatic relapse in the absence of primary tumor. Finally, of the tested E0771 and LLC cancer models, the latter is known to be unresponsive to traditional anti-angiogenic therapies such as VEGF(R) inhibitors[53, 54].

The observation that B55α was not detectable in fully mature and stabilized blood vessels of adult organs, and that mural cell-covered tumor blood vessels were still detectable in B55α^{iEC-KO} (or LB100-treated) mice, lead to additional clinical speculations. Firstly, B55α/PP2A blockers or pan-PP2A inhibitors affect only remodeling blood vessels whereas VEGF(R) inhibitors mainly target hyperactive ECs. Yet, B55α/PP2A blockers or pan-PP2A inhibitors would spare mature vessels, which are the routes for anti-cancer drugs into the tumor[12]. In healthy organs, disturbance of blood vessel homeostasis causes severe side effects[17] as observed in the clinical use of anti-VEGF(R) drugs[20, 26, 55]. Thus, B55α/PP2A inhibition could tackle pathological blood vessels more selectively than current anti-angiogenic drugs. In an opposite scenario, our data predicts that overactivation of the B55α/PP2A complex might protect blood vessels against oxidative stress, an important issue which could be explored in disease settings such as ischemic repercussion injury.

ACKNOWLEDGEMENTS
We thank Tanja Rothgangl, Federica Diofano, Lena Burchhart, Jens Serneels, Sarah Trusso Cafarello, Mohamed Mahmoud Saad and Eline Achten for excellent technical assistance.

SOURCES OF FUNDING
M.E. was supported by the Deutsche Forschungsgemeinschaft (EH 472/1-1), Kom op tegen Kanker (Stand up to Cancer), and the Flemish cancer society (2016/10538/2453), W.C. by an FWO-Strategic Basis Research (SB) doctoral fellowship (1S26917N), R.M.P. by FWO, R.A.R. by FPI associated to SAF 2017/88275-R, E.A.V.J. by FWO (G091018N) and KU Leuven (IDN/19/031, C14-19_095) and G.D.C. by a Pegasus FWO-Marie Curie fellowship (12114113N). M.M. received an ERC consolidator grant (773208) and FWO grant (G0D1717N).

DISCLOSURES
None.

SUPPLEMENTAL MATERIALS
Expanded Materials & Methods
Online Figures I - VIII
Online Data Table I
Unedited Gels
Major Resources Table

REFERENCES

1. Adams RH and Alitalo K. Molecular regulation of angiogenesis and lymphangiogenesis. *Nat Rev Mol Cell Biol*. 2007;8:464-78.
2. Ehling M, Adams S, Benedito R and Adams RH. Notch controls retinal blood vessel maturation and quiescence. *Development*. 2013;140:3051-61.
3. Mukouyama YS, Shin D, Britsch S, Taniguchi M and Anderson DJ. Sensory nerves determine the pattern of arterial differentiation and blood vessel branching in the skin. *Cell*. 2002;109:693-705.
4. Watson EC, Koenig MN, Grant ZL, Whitehead L, Trounson E, Dewson G and Coultas L. Apoptosis regulates endothelial cell number and capillary vessel diameter but not vessel regression during retinal angiogenesis. *Development*. 2016;143:2973-82.
5. Franco CA, Jones ML, Bernabeu MO, Geudens I, Mathivet T, Rosa A, Lopes FM, Lima AP, Ragab A, Collins RT, Phng LK, Coveney PV and Gerhardt H. Dynamic endothelial cell rearrangements drive developmental vessel regression. *PLoS Biol*. 2015;13:e1002125.
6. Xu C, Hasan SS, Schmidt I, Rocha SF, Pitulescu ME, Bussmann J, Meyen D, Raz E, Adams RH and Siekmann AF. Arteries are formed by vein-derived endothelial tip cells. *Nat Commun*. 2014;5:5758.
7. Carmeliet P. Angiogenesis in health and disease. *Nat Med*. 2003;9:653-60.
8. Baeyens N, Bandyopadhyay C, Coon BG, Yun S and Schwartz MA. Endothelial fluid shear stress sensing in vascular health and disease. *J Clin Invest*. 2016;126:821-8.
9. Staiculescu MC, Foote C, Meininger GA and Martinez-Lemus LA. The role of reactive oxygen species in microvascular remodeling. *Int J Mol Sci*. 2014;15:23792-835.
10. Santoro MM. Fashioning blood vessels by ROS signalling and metabolism. *Semin Cell Dev Biol*. 2018;80:35-42.
11. Korn C and Augustin HG. Mechanisms of Vessel Pruning and Regression. *Dev Cell*. 2015;34:5-17.
12. Leite de Oliveira R, Deschoemaeker S, Henze AT, Debackere K, Finisguerra V, Takeda Y, Roncal C, Dettori D, Tack E, Jonsson Y, Veschini L, Peeters A, Anisimov A, Hofmann M, Alitalo K, Baes M,

D'Hooge J, Carmeliet P and Mazzone M. Gene-targeting of Phd2 improves tumor response to chemotherapy and prevents side-toxicity. *Cancer Cell*. 2012;22:263-77.
13. Kapitsinou PP, Sano H, Michael M, Kobayashi H, Davidoff O, Bian A, Yao B, Zhang MZ, Harris RC, Duffy KJ, Erickson-Miller CL, Sutton TA and Haase VH. Endothelial HIF-2 mediates protection and recovery from ischemic kidney injury. *J Clin Invest*. 2014;124:2396-409.
14. Scortegagna M, Ding K, Oktay Y, Gaur A, Thurmond F, Yan LJ, Marck BT, Matsumoto AM, Shelton JM, Richardson JA, Bennett MJ and Garcia JA. Multiple organ pathology, metabolic abnormalities and impaired homeostasis of reactive oxygen species in Epas1-/- mice. *Nat Genet*. 2003;35:331-40.
15. Corre I, Paris F and Huot J. The p38 pathway, a major pleiotropic cascade that transduces stress and metastatic signals in endothelial cells. *Oncotarget*. 2017;8:55684-55714.
16. Ferrara N, Gerber HP and LeCouter J. The biology of VEGF and its receptors. *Nat Med*. 2003;9:669-76.
17. Lee S, Chen TT, Barber CL, Jordan MC, Murdock J, Desai S, Ferrara N, Nagy A, Roos KP and Iruela-Arispe ML. Autocrine VEGF signaling is required for vascular homeostasis. *Cell*. 2007;130:691-703.
18. Ribatti D, Annese T, Ruggieri S, Tamma R and Crivellato E. Limitations of Anti-Angiogenic Treatment of Tumors. *Transl Oncol*. 2019;12:981-986.
19. Hurwitz H, Fehrenbacher L, Novotny W, Cartwright T, Hainsworth J, Heim W, Berlin J, Baron A, Griffing S, Holmgren E, Ferrara N, Fyfe G, Rogers B, Ross R and Kabbinavar F. Bevacizumab plus irinotecan, fluorouracil, and leucovorin for metastatic colorectal cancer. *N Engl J Med*. 2004;350:2335-42.
20. Loges S, Mazzone M, Hohensinner P and Carmeliet P. Silencing or fueling metastasis with VEGF inhibitors: antiangiogenesis revisited. *Cancer Cell*. 2009;15:167-70.
21. Eichhorn PJ, Creyghton MP and Bernards R. Protein phosphatase 2A regulatory subunits and cancer. *Biochim Biophys Acta*. 2009;1795:1-15.
22. Di Conza G, Trusso Cafarello S, Loroch S, Mennerich D, Deschoemaeker S, Di Matteo M, Ehling M, Gevaert K, Prenen H, Zahedi RP, Sickmann A, Kietzmann T, Moretti F and Mazzone M. The mTOR and PP2A Pathways Regulate PHD2 Phosphorylation to Fine-Tune HIF1alpha Levels and Colorectal Cancer Cell Survival under Hypoxia. *Cell Rep*. 2017;18:1699-1712.
23. Di Conza G, Trusso Cafarello S, Zheng X, Zhang Q and Mazzone M. PHD2 Targeting Overcomes Breast Cancer Cell Death upon Glucose Starvation in a PP2A/B55alpha-Mediated Manner. *Cell Rep*. 2017;18:2836-2844.
24. Martin M, Geudens I, Bruyr J, Potente M, Bleuart A, Lebrun M, Simonis N, Deroanne C, Twizere JC, Soubeyran P, Peixoto P, Mottet D, Janssens V, Hofmann WK, Claes F, Carmeliet P, Kettmann R, Gerhardt H and Dequiedt F. PP2A regulatory subunit Balpha controls endothelial contractility and vessel lumen integrity via regulation of HDAC7. *EMBO J*. 2013;32:2491-503.
25. Yamamoto H, Ehling M, Kato K, Kanai K, van Lessen M, Frye M, Zeuschner D, Nakayama M, Vestweber D and Adams RH. Integrin beta1 controls VE-cadherin localization and blood vessel stability. *Nat Commun*. 2015;6:6429.
26. De Bock K, Mazzone M and Carmeliet P. Antiangiogenic therapy, hypoxia, and metastasis: risky liaisons, or not? *Nat Rev Clin Oncol*. 2011;8:393-404.
27. Steeg PS. Tumor metastasis: mechanistic insights and clinical challenges. *Nat Med*. 2006;12:895-904.
28. Hong CS, Ho W, Zhang C, Yang C, Elder JB and Zhuang Z. LB100, a small molecule inhibitor of PP2A with potent chemo- and radio-sensitizing potential. *Cancer Biol Ther*. 2015;16:821-33.
29. Chung V, Mansfield AS, Braiteh F, Richards D, Durivage H, Ungerleider RS, Johnson F and Kovach JS. Safety, Tolerability, and Preliminary Activity of LB-100, an Inhibitor of Protein Phosphatase 2A, in Patients with Relapsed Solid Tumors: An Open-Label, Dose Escalation, First-in-Human, Phase I Trial. *Clin Cancer Res*. 2017;23:3277-3284.
30. https://clinicaltrials.gov/ct2/results?cond=&term=LB100&cntry=&state=&city=&dist
31. Deskins DL, Ardestani S and Young PP. The polyvinyl alcohol sponge model implantation. *J Vis Exp*. 2012.

32. Kalucka J, Bierhansl L, Conchinha NV, Missiaen R, Elia I, Bruning U, Scheinok S, Treps L, Cantelmo AR, Dubois C, de Zeeuw P, Goveia J, Zecchin A, Taverna F, Morales-Rodriguez F, Brajic A, Conradi LC, Schoors S, Harjes U, Vriens K, Pilz GA, Chen R, Cubbon R, Thienpont B, Cruys B, Wong BW, Ghesquiere B, Dewerchin M, De Bock K, Sagaert X, Jessberger S, Jones EAV, Gallez B, Lambrechts D, Mazzone M, Eelen G, Li X, Fendt SM and Carmeliet P. Quiescent Endothelial Cells Upregulate Fatty Acid beta-Oxidation for Vasculoprotection via Redox Homeostasis. *Cell Metab*. 2018;28:881-894 e13.
33. Noseda M, Chang L, McLean G, Grim JE, Clurman BE, Smith LL and Karsan A. Notch activation induces endothelial cell cycle arrest and participates in contact inhibition: role of p21Cip1 repression. *Mol Cell Biol*. 2004;24:8813-22.
34. Scortegagna M, Ding K, Zhang Q, Oktay Y, Bennett MJ, Bennett M, Shelton JM, Richardson JA, Moe O and Garcia JA. HIF-2alpha regulates murine hematopoietic development in an erythropoietin-dependent manner. *Blood*. 2005;105:3133-40.
35. Scortegagna M, Morris MA, Oktay Y, Bennett M and Garcia JA. The HIF family member EPAS1/HIF-2alpha is required for normal hematopoiesis in mice. *Blood*. 2003;102:1634-40.
36. Mazzone M, Dettori D, Leite de Oliveira R, Loges S, Schmidt T, Jonckx B, Tian YM, Lanahan AA, Pollard P, Ruiz de Almodovar C, De Smet F, Vinckier S, Aragones J, Debackere K, Luttun A, Wyns S, Jordan B, Pisacane A, Gallez B, Lampugnani MG, Dejana E, Simons M, Ratcliffe P, Maxwell P and Carmeliet P. Heterozygous deficiency of PHD2 restores tumor oxygenation and inhibits metastasis via endothelial normalization. *Cell*. 2009;136:839-51.
37. Asada S, Daitoku H, Matsuzaki H, Saito T, Sudo T, Mukai H, Iwashita S, Kako K, Kishi T, Kasuya Y and Fukamizu A. Mitogen-activated protein kinases, Erk and p38, phosphorylate and regulate Foxo1. *Cell Signal*. 2007;19:519-27.
38. Yang Y, Cai X, Yang J, Sun X, Hu C, Yan Z, Xu X, Lu W, Wang X and Cao P. Chemoprevention of dietary digitoflavone on colitis-associated colon tumorigenesis through inducing Nrf2 signaling pathway and inhibition of inflammation. *Mol Cancer*. 2014;13:48.
39. Chen D, Reierstad S, Lin Z, Lu M, Brooks C, Li N, Innes J and Bulun SE. Prostaglandin E(2) induces breast cancer related aromatase promoters via activation of p38 and c-Jun NH(2)-terminal kinase in adipose fibroblasts. *Cancer Res*. 2007;67:8914-22.
40. Wang Y, Xia Y, Kuang D, Duan Y and Wang G. PP2A regulates SCF-induced cardiac stem cell migration through interaction with p38 MAPK. *Life Sci*. 2017;191:59-67.
41. Joseph BK, Liu HY, Francisco J, Pandya D, Donigan M, Gallo-Ebert C, Giordano C, Bata A and Nickels JT, Jr. Inhibition of AMP Kinase by the Protein Phosphatase 2A Heterotrimer, PP2APpp2r2d. *J Biol Chem*. 2015;290:10588-98.
42. Arriazu E, Pippa R and Odero MD. Protein Phosphatase 2A as a Therapeutic Target in Acute Myeloid Leukemia. *Front Oncol*. 2016;6:78.
43. Schulte-Merker S, Sabine A and Petrova TV. Lymphatic vascular morphogenesis in development, physiology, and disease. *J Cell Biol*. 2011;193:607-18.
44. Morfoisse F, Renaud E, Hantelys F, Prats AC and Garmy-Susini B. Role of hypoxia and vascular endothelial growth factors in lymphangiogenesis. *Mol Cell Oncol*. 2015;2:e1024821.
45. Casazza A, Di Conza G, Wenes M, Finisguerra V, Deschoemaeker S and Mazzone M. Tumor stroma: a complexity dictated by the hypoxic tumor microenvironment. *Oncogene*. 2014;33:1743-54.
46. Scallan J, Huxley VH and Korthuis RJ. *Capillary Fluid Exchange: Regulation, Functions, and Pathology* San Rafael (CA); 2010.
47. Yun S, Hu R, Schwaemmle ME, Scherer AN, Zhuang Z, Koleske AJ, Pallas DC and Schwartz MA. Integrin alpha5beta1 regulates PP2A complex assembly through PDE4D in atherosclerosis. *J Clin Invest*. 2019;130.
48. Watson EC, Grant ZL and Coultas L. Endothelial cell apoptosis in angiogenesis and vessel regression. *Cell Mol Life Sci*. 2017;74:4387-4403.

49. Skuli N, Majmundar AJ, Krock BL, Mesquita RC, Mathew LK, Quinn ZL, Runge A, Liu L, Kim MN, Liang J, Schenkel S, Yodh AG, Keith B and Simon MC. Endothelial HIF-2alpha regulates murine pathological angiogenesis and revascularization processes. *J Clin Invest*. 2012;122:1427-43.
50. Zarubin T and Han J. Activation and signaling of the p38 MAP kinase pathway. *Cell Res*. 2005;15:11-8.
51. Ferrari G, Terushkin V, Wolff MJ, Zhang X, Valacca C, Poggio P, Pintucci G and Mignatti P. TGF-beta1 induces endothelial cell apoptosis by shifting VEGF activation of p38(MAPK) from the prosurvival p38beta to proapoptotic p38alpha. *Mol Cancer Res*. 2012;10:605-14.
52. Mudgett JS, Ding J, Guh-Siesel L, Chartrain NA, Yang L, Gopal S and Shen MM. Essential role for p38alpha mitogen-activated protein kinase in placental angiogenesis. *Proc Natl Acad Sci U S A*. 2000;97:10454-9.
53. Casazza A, Fu X, Johansson I, Capparuccia L, Andersson F, Giustacchini A, Squadrito ML, Venneri MA, Mazzone M, Larsson E, Carmeliet P, De Palma M, Naldini L, Tamagnone L and Rolny C. Systemic and targeted delivery of semaphorin 3A inhibits tumor angiogenesis and progression in mouse tumor models. *Arterioscler Thromb Vasc Biol*. 2011;31:741-9.
54. Shojaei F, Wu X, Malik AK, Zhong C, Baldwin ME, Schanz S, Fuh G, Gerber HP and Ferrara N. Tumor refractoriness to anti-VEGF treatment is mediated by CD11b+Gr1+ myeloid cells. *Nat Biotechnol*. 2007;25:911-20.
55. Kamba T and McDonald DM. Mechanisms of adverse effects of anti-VEGF therapy for cancer. *Br J Cancer*. 2007;96:1788-95.
56. Cao J, Ehling M, Marz S, Seebach J, Tarbashevich K, Sixta T, Pitulescu ME, Werner AC, Flach B, Montanez E, Raz E, Adams RH and Schnittler H. Polarized actin and VE-cadherin dynamics regulate junctional remodelling and cell migration during sprouting angiogenesis. Nat Commun. 2017;8:2210.
57. Subramanian A, Tamayo P, Mootha VK, Mukherjee S, Ebert BL, Gillette MA, Paulovich A, Pomeroy SL, Golub TR, Lander ES and Mesirov JP. Gene set enrichment analysis: a knowledge-based approach for interpreting genome-wide expression profiles. Proc Natl Acad Sci U S A. 2005;102:15545-50.
58. Lallemand Y, Luria V, Haffner-Krausz R and Lonai P. Maternally expressed PGK-Cre transgene as a tool for early and uniform activation of the Cre site-specific recombinase. Transgenic Res. 1998;7:105-12.
59. Farley FW, Soriano P, Steffen LS and Dymecki SM. Widespread recombinase expression using FLPeR (flipper) mice. Genesis. 2000;28:106-10.
60. Clausen BE, Burkhardt C, Reith W, Renkawitz R and Forster I. Conditional gene targeting in macrophages and granulocytes using LysMcre mice. Transgenic Res. 1999;8:265-77.
61. Jullien N, Goddard I, Selmi-Ruby S, Fina JL, Cremer H and Herman JP. Use of ERT2-iCre-ERT2 for conditional transgenesis. Genesis. 2008;46:193-9.
62. Wang Y, Nakayama M, Pitulescu ME, Schmidt TS, Bochenek ML, Sakakibara A, Adams S, Davy A, Deutsch U, Luthi U, Barberis A, Benjamin LE, Makinen T, Nobes CD and Adams RH. Ephrin-B2 controls VEGF-induced angiogenesis and lymphangiogenesis. Nature. 2010;465:483-6.
63. Bazigou E, Xie S, Chen C, Weston A, Miura N, Sorokin L, Adams R, Muro AF, Sheppard D and Makinen T. Integrin-alpha9 is required for fibronectin matrix assembly during lymphatic valve morphogenesis. Dev Cell. 2009;17:175-86.
64. Ved N, Curran A, Ashcroft FM and Sparrow DB. Tamoxifen administration in pregnant mice can be deleterious to both mother and embryo. Lab Anim. 2019;53:630-633.

FIGURE LEGENDS

Figure 1: B55α expression is essential for embryonic development.
(A) Analysis of B55α protein and mRNA sequences between species. **(B)** Expression of B55α in embryonic tissue at day 14.5 post fertilization (=E14.5) assessed by RNAscope. Scale bars: 1000µm in the overviews and 50µm in the higher resolution images. **(C-E)** Analysis of B55α protein (n=5 per group) and mRNA expression (Ctrl n=4; Het n=6; Hom n=4) levels in control and KO embryos at E12.5. **(F)** Ratio of surviving B55α-KO embryos at different stages of development. **(G)** Representative images of controls and *Ppp2r2a* Full-KO embryos at embryonic stage E14.5. White arrows indicate visible bleedings in the skin of mutant embryos. **(H,J,L)** Representative images of embryonic skin samples from *Ppp2r2a* Full-KO and littermate controls stained for $CD31^+$ blood vessels **(H)** Collagen IV^+ / $CD31^-$ empty sleeves as a marker for pruned blood vessels **(J)** and $Lyve1^+$ lymph vessels **(L)**. Scale bars: 100 µm. **(I,K,M)** Quantitative analysis of $CD31^+$ blood vessel area (Ctrl n=5; Het n=5; Hom n=3) **(I)** Collagen IV^+ / $CD31^-$ pruning blood vessels (Ctrl n=7; Het n=7; Hom n=6) **(K)**, and $Lyve1^+$ lymph vessel area (Ctrl n=7; Het n=7; Hom n=6) **(M)** in surviving embryos at stage E14.5. One-way ANOVA followed by Tukey test was performed in **(D)**, **(E)**, **(I)**, **(K)** and **(M)**. Graphs show standard SEM.

Figure 2: Endothelial loss of B55α leads to vascular and lymphatic defects resulting in embryonic lethality. (A) Representative images of E14.5 embryos lacking endothelial B55α and littermate controls. Black arrows indicate bleedings in the skin of mutant embryos. **(B-D)** Whole mount skin samples stained for lymph vessel marker Lyve1 **(C)** and the blood vessel marker CD31 **(D)**. Scale bars: 200µm. **(E,F)** Quantitative analysis of lymph vessel diameter (n=4 embryos per group) **(E)** and blood vessel density in the remodeling vascular plexus (Ctrl n=26; $B55\alpha^{iEC\text{-}KO}$ n=12) **(F)**. **(G,I)** Apoptotic ECs in the remodeling vascular plexus indicated by immunostainings against CD31 and cleaved Caspase3 **(G)** and quantitative analysis thereof (Ctrl n=18; $B55\alpha^{iEC\text{-}KO}$ n=9) **(I)** Scale bar: 100µm. **(H,J)** Pruning blood vessels, visualized by Co-staining of $CD31^+$ and CollagenIV^+ / $CD31^-$ empty sleeves **(H)** and quantitative analysis thereof (n=4 per group) **(J)** Scale bar: 100µm. **(K)** Representative images of whole embryos at stage E16.5 and statistical quantification thereof. **(L-O)** Representative images of embryonic skin samples at stage E16.5 stained for $CD31^+$ blood vessels **(L)** and $Lyve1^+$ lymph vessels **(N)** and statistical analysis thereof (n=9 per group in **(M)** and n=4 per group in **(O)**). Scale bars: 200µm. Unpaired t-tests were performed in **(E)**, **(F)**, **(I)**, **(J)**, **(M)** and **(O)**. Graphs show SEM.

Figure 3: Deletion of B55α in the tumor vasculature delays tumor progression, by reducing the blood vessel density.
(A-F) Tumor progression after EC specific deletion of *Ppp2r2a* following the subcutaneous injection of LLC cancer cells (Ctrl n=19; $B55\alpha^{iEC\text{-}KO}$ n=8) **(A)**, tumor weight (Ctrl n=18; $B55\alpha^{iEC\text{-}KO}$ n=11) **(B)** and lung metastasis (Ctrl n=40; $B55\alpha^{iEC\text{-}KO}$ n=30) **(C).** Tumor progression after EC specific deletion of *Ppp2r2a* following orthotopically injected E0771 breast cancer cells (Ctrl n=9; $B55\alpha^{iEC\text{-}KO}$ n=14) **(D)**, tumor weight (Ctrl n=12; $B55\alpha^{iEC\text{-}KO}$ n=7) **(E)** and lung metastasis (Ctrl n=33; $B55\alpha^{iEC\text{-}KO}$ n=36) **(F)**. **(G-J)** Representative images and quantifications of hypoxic areas in LLC (Ctrl n=13; $B55\alpha^{iEC\text{-}KO}$ n=8) **(G,H)** and E0771 tumors (Ctrl n=8; $B55\alpha^{iEC\text{-}KO}$ n=9). **(I,J)** Scale bars: 100µm. **(K-N)** Representative images and quantifications and of necrotic areas in LLC (n=19 per group) **(K,L)** and E0771 tumors (Ctrl n=8; $B55\alpha^{iEC\text{-}KO}$ n=7) **(M,N)**. Scale bars: 400µm. **(O-X)** 70µm thick cryosections of LLC **(O,S)** and E0771 **(Q,V)** tumors stained for $CD31^+$ blood vessels and the apoptosis marker cleaved Caspase3 and statistical analysis of blood vessel density **(P,R)**, total area of apoptotic (tumor) areas **(T,W)** and cleaved $Caspase3^+$ ECs **(U,X)**; (n=7 per group) **(P,T,U)** and (Ctrl n=6; $B55\alpha^{iEC\text{-}KO}$ n=7) **(R,W,X)**. Scale bars: 100µm **(O,Q)**, 10µm **(S,V)**.
Unpaired t-tests were performed in **(B)**, **(E)**, **(F)**, **(H)**, **(J)**, **(N)**, **(P)**, **(R)**, **(T)**, **(U)**, **(W)** a non-parametric Mann-Whitney tests in **(C)**, **(F)**, **(L)** **(X)** and a two-way repeated measures ANOVA in **(A)** and **(D)**.
Graphs show SEM.

Figure 4: Deletion of endothelial B55α after tumor resection delays metastatic growth and prolongs survival of mutant mice.
(A) Schematic layout of the depicted experiment. **(B)** Tumor size at the day of tumor resection. **(C)** Quantitative analysis showing survival of littermate controls and mutant mice after tumor resection and subsequent tamoxifen induced depletion of endothelial *Ppp2r2a*. **(D)** Quantitative analysis of the number of lung metastasis. **(E,F)** Representative images of metastatic lungs from controls and mutant mice **(E)** and quantitative analysis thereof **(F)**. Scale bar: 5mm**. (G,H)** Representative images of H&E stained lungs showing dense metastatic nodules within normal lung tissue **(G)** and the quantitative analysis thereof **(H)**. Scale bar: 5mm. **(I,J)** Representative images showing the vasculature within lung metastasis in controls and mutant mice **(I)** and quantitative analysis thereof **(J).** Scale bar: 200µm. (Ctrl n=11; B55α$^{iEC\text{-}KO}$ n=8 for all panels). Unpaired t-tests were performed in **(B)**, **(D)**, **(F)**, **(H)** and **(J)**. Graphs show SEM.

Figure 5: Chemical pan-PP2A inhibition induces blood vessel pruning and delays tumor progression.
(A) Schematic representation of the sponge implantation assay shown in **(B,C) (B,C)** Representative images of sponges stained for CD31^{+} blood vessels. Scale bar: 100µm. **(B)** and quantitative analysis thereof (Ctrl n=7; B55α$^{iEC\text{-}KO}$ n=9 for each dose of LB100) **(C)**. **(D-F)** Subcutaneous LLC tumor growth **(D)**, final tumor burden **(E)** and body weight **(F)** in B55α$^{iEC\text{-}KO}$ mutant or after systemic LB100 treatment (alone and in combination). **(G, H)** 6µm thin paraffin sections of tumor samples stained for CD31+ blood vessels **(G)** and statistical analysis of blood vessel density **(H)**. Scale bars: 100µm. **(I, J)** Representative images **(I)** and quantifications **(J)** of pimonidazole-positive tumor areas, indicating hypoxic regions. Scale bar: 200µm.
Ctrl(PBS) n=5; Ctrl(LB100) n=5; B55α$^{iEC\text{-}KO}$ (PBS) n=4; B55□$^{iEC\text{-}KO}$ (LB100) n=5 in **(D-H)**. One-way ANOVA followed by Tukey test was performed in **(C)**, **(E)**, **(H)**, **(J)** and a two-way repeated measures ANOVA in **(D)** and **(F)**. Graphs show SEM.

Figure 6: B55a is upregulated in densely seeded HUVECs and prevents apoptosis induction.
(A,B) Analysis of B55α RNA **(A)** and protein level **(B)** in HUVECs cultured at different cell densities.
(C) Survival analysis of HUVECs after KD of B55α. **(D,E)** Analysis of apoptosis in B55α-KD and LB100 treated HUVECs by subG1 FACS assay performed on fixed samples **(D)** and AnnexinV/PI FACS assay performed on living ECs **(E)**. **(F)** WB analysis of cleaved PARP in B55α-KD HUVECs. **(G-I)** Immunostainings of B55α-KD HUVECs treated with vehicle control (NT), pan-Caspase inhibitors (qVD or zVAD) for Phalloidin, cleaved Caspase3 and Hoechst **(G)** and quantitative analysis thereof **(H-I).** Scale bar: 100µm. **(J)** Schematic representation of the experiments depicted in **(K)** and **(L)**. **(K,L)** Analysis of cell survival after KD of B55α in spares and dense HUVECs. **(M)** Analysis of cell survival in spares and dense HUVECs treated with the pan-PP2A inhibitor LB100.

n=3 per group in **(A)**, **(E)**, **(K)**, **(L)**, **(M)**, n=5 per group in **(H)**, **(I)** and n=6 per group in **(C)** and **(D)**.
Unpaired t-tests were performed in **(D)**, one-way ANOVA followed by Tukey test in **(A)**, **(E)**, **(F)**, **(H)**, **(I)**, **(K)**, **(L)**, **(M)** and a two-way repeated measures ANOVA in **(C)**.
Graphs show SEM.

Figure 7: B55α expression counteracts ROS and cell stress in a PHD dependent manner.
(A) WBs showing B55α expression in presence of the ROS scavenger MnTBAP. **(B, C)** CM-H2DCFDA-based ROS assay analyzing H_2O_2-induced ROS on sparse, confluent and dense HUVECs (n=3 per group) **(B)** qVD-treated B55α-KD HUVECs under dense conditions (n=6 per group) **(C)**. **(D-F)** WB analysis of HIF1α, HIF2α, p-AKT **(D)**, the cell stress indicators p-eIF2α, p21, the apoptosis marker cleaved Caspase3 **(E)**, B55α and p-p38 **(F)** in B55α-KD and controls upon DMOG treatment. **(G)** qPCR-based expression analysis of B55α in sparse and dense HUVECs upon H_2O_2 treatment (Sparse n=5; Dense n=6 per treatment group). **(H,I)** qPCR-based expression analysis of B55α **(H)** and genes counteracting ROS and EC maturation markers such as total FLT1 and CDH5 **(I)** in control and B55α-KD cells and in combination with DMOG treatment (n=3 per group). Significance was calculated on log2 transformed data followed by

two-way ANOVA. **(J-L)** Staining of Phalloidin and Hoechst in DMOG treated B55α-KD and control HUVECs **(J)**, quantification of resistance to H_2O_2 (n=3 per group) **(K)** and cell survival (n=15 per group) **(L).** Scale bar: 100µm. **(M,N)** Representative images of sponges stained for $CD31^+$ blood vessels **(M)** and quantification thereof (n=6 per group) **(N)**. Scale bar: 300µm. One-way ANOVA followed by Tukey test was performed in **(G), (H), (K), (L)**, **(N)** and a two-way repeated measures ANOVA in **(B)** and **(C)**.
Graphs show SEM.

Figure 8: B55α blocks the prolonged and apoptosis inducing activity of p38.
(A) WB analysis of p-p38 after KD of B55α. **(B)** Co-IP experiments of B55α and p38 performed in dense HUVECs. **(C,D)** Ctrl and B55α-KD HUVECs treated with p38 inhibitor and stained for Phalloidin and Hoechst **(C)** and quantification thereof (n≥11 per group) **(D)**. Scale bar: 100µm. **(E)** Schematic representation of p38 control on EC apoptosis, explaining the results of the experiments depicted in **(D)** and **(G)**. **(F-H)** Immunostainings for $CD31^+$ blood vessels of implanted sponges derived from control and $B55\alpha^{iEC\text{-}KO}$ mice treated with p38 inhibitor **(F)**, and quantification thereof (Ctrl n=9; $B55\alpha^{iEC\text{-}KO}$ n=7 for each dose of p38 inhibitor) **(G,H)**. Scale bar: 300µm. **(I)** Graphical abstract summarizing our findings and the proposed mechanism. An unpaired t-test was performed in **(H)** and One-way-Anova followed by Tukey test in **(D)** and **(G)**.
Graphs show SEM.

NOVELTY AND SIGNIFICANCE

What Is Known?

- VEGF and other signaling molecules have been implicated in vessel growth. Though the signaling that regulates remodeling of nascent vascular networks is poorly characterized.
- Many progressing tumors do not respond or develop resistance to VEGF-targeted antiangiogenic therapies, resulting in limited success during clinical applications.
- Inhibition of the B55α/PP2A complex in cancer cells alleviates tumor progression by reducing cell viability in response to hypoxia and glucose starvation.

What New Information Does This Article Contribute?

- During both development and adult life (*i.e.* in cancer), B55α/PP2A elicits a HIF- and p38-dependent survival program during vascular remodeling that protects ECs in nascent blood vessels against oxidative and other flow-related cell stress.
- Deletion of B55α/PP2A has no effect in healthy adult mice or fully mature blood vessels.
- B55α/PP2A inhibitors can be exploited as potential anti-angiogenic cancer therapies that work in a complementary manner to anti-VEGF drugs, offering an alternative in case of resistance to these therapies.

We have previously shown that inhibition of the B55α/PP2A phosphatase complex delays tumor progression by inducing cancer cell apoptosis in response to oxygen or glucose restriction. These findings underline the potential use of B55α/PP2A phosphatase blockers for cancer therapy. Yet, little is known on the role of B55α/PP2A in the tumor stroma and particularly in the blood vessels. Moreover, possible side effects due to systemic inhibition of B55α/PP2A remain understudied.

Here we generated novel transgenic mice to induce genetic deletion of B55α in different cell types and at specific timepoints of cancer progression. We found that neither ubiquitous nor endothelial cell specific deletion of B55α had effects in healthy adult mice or more specifically, on established, quiescent blood vessels. In contrast, genetic deletion of B55α or chemical inhibition of PP2A unleashed strong pruning effects of the immature tumor vasculature and thereby delayed cancer and metastatic progression. The identified mechanism is complementary to currently used anti-angiogenic drugs, suggesting that B55α/PP2A phosphatase inhibition could serve as an alternative strategy in case tumors become resistant or do not respond to state-of-the-art anti-angiogenic agents.

Taken together, our study argues that targeting the B55α/PP2A complex might be a safe and powerful approach for clinical applications.

Figure 1

A

Species	Conservation	
Homo sapiens	Protein	mRNA
vs. Pan troglodytes	100.0 %	99.9 %
vs. Canis lupus	99.6 %	96.6 %
vs. Bos taurus	99.3 %	96.5 %
vs. Mus musculus	100.0 %	93.9 %
vs. Rattus norvegicus	99.8 %	93.0 %
vs. Gallus gallus	99.3 %	89.1 %
vs. Xenopus tropicalis	94.8 %	78.4 %
vs. Danio rerio	92.0 %	78.0 %

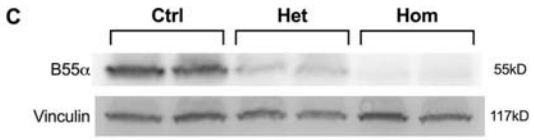

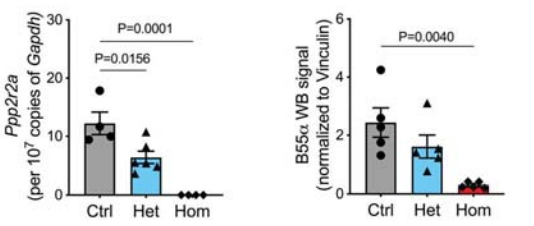

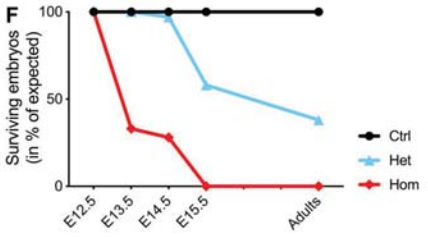

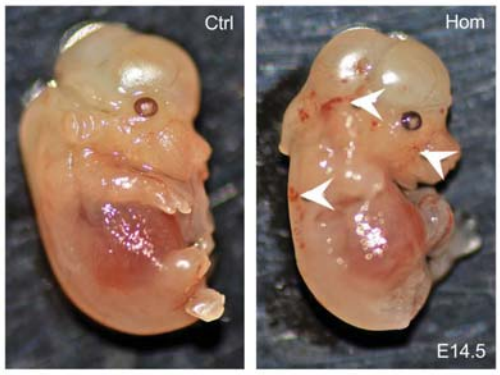

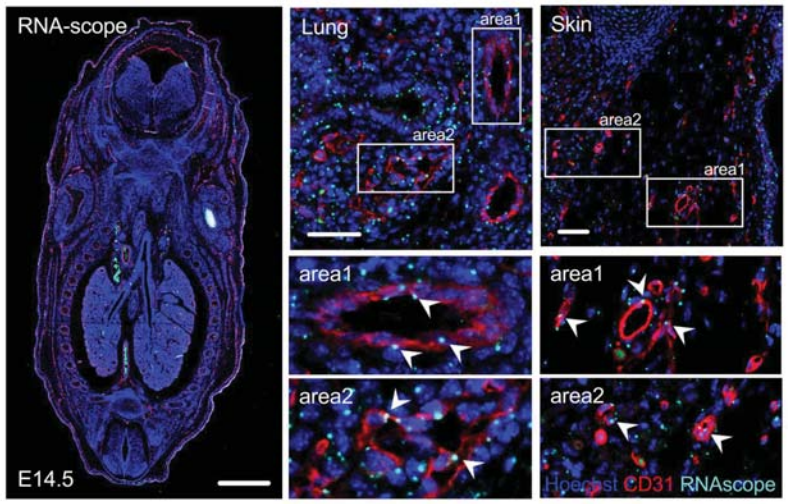

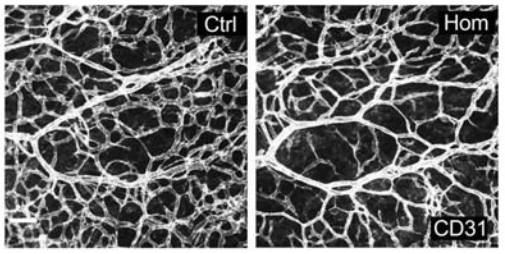

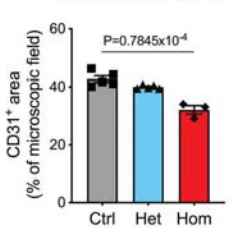

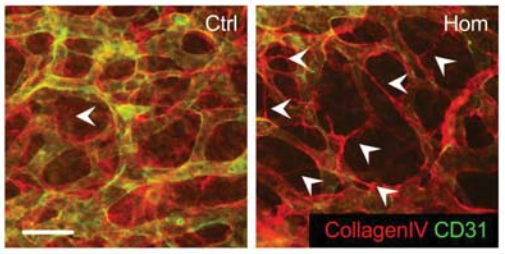

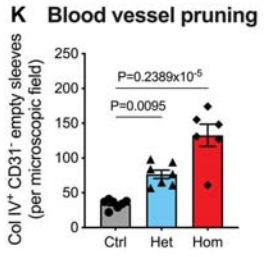

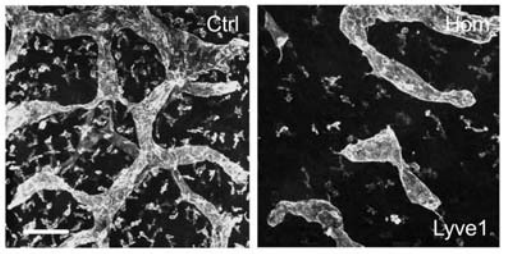

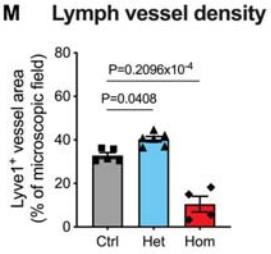

Figure 2

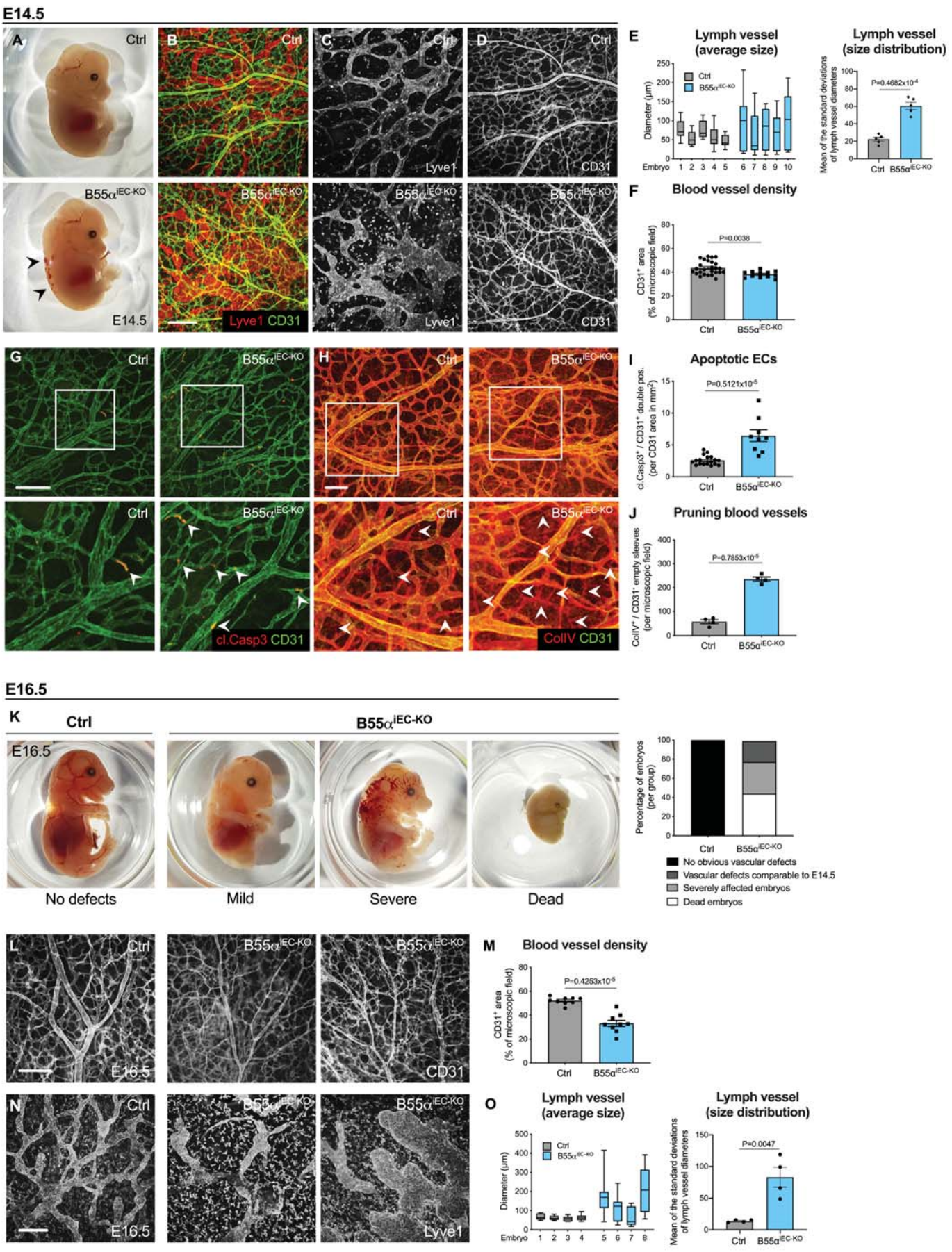
E14.5
A
Ctrl
B
Ctrl
C
Ctrl
Lyve1
D
Ctrl
CD31
B55α iEC-KO
E14.5
B55α iEC-KO
Lyve1 CD31
B55α iEC-KO
Lyve1
B55α iEC-KO
CD31
E
Lymph vessel (average size)
Diameter (µm)
Ctrl
B55α iEC-KO
Embryo 1 2 3 4 5 6 7 8 9 10
Lymph vessel (size distribution)
Mean of the standard deviations of lymph vessel diameters
P=0.4682x10-4
Ctrl
B55α iEC-KO
F
Blood vessel density
CD31+ area (% of microscopic field)
P=0.0038
Ctrl
B55α iEC-KO
G
Ctrl
B55α iEC-KO
H
Ctrl
B55α iEC-KO
Ctrl
B55α iEC-KO
cl.Casp3 CD31
Ctrl
B55α iEC-KO
ColIV CD31
I
Apoptotic ECs
cl.Casp3+ / CD31+ double pos. (per CD31 area in mm2)
P=0.5121x10-5
Ctrl
B55α iEC-KO
J
Pruning blood vessels
ColIV+ / CD31- empty sleeves (per microscopic field)
P=0.7853x10-5
Ctrl
B55α iEC-KO
E16.5
K
Ctrl
B55α iEC-KO
E16.5
No defects
Mild
Severe
Dead
Percentage of embryos (per group)
Ctrl
B55α iEC-KO
No obvious vascular defects
Vascular defects comparable to E14.5
Severely affected embryos
Dead embryos
L
Ctrl
E16.5
B55α iEC-KO
B55α iEC-KO
CD31
M
Blood vessel density
CD31+ area (% of microscopic field)
P=0.4253x10-5
Ctrl
B55α iEC-KO
N
Ctrl
E16.5
B55α iEC-KO
B55α iEC-KO
Lyve1
O
Lymph vessel (average size)
Diameter (µm)
Ctrl
B55α iEC-KO
Embryo 1 2 3 4 5 6 7 8
Lymph vessel (size distribution)
Mean of the standard deviations of lymph vessel diameters
P=0.0047
Ctrl
B55α iEC-KO

Figure 3

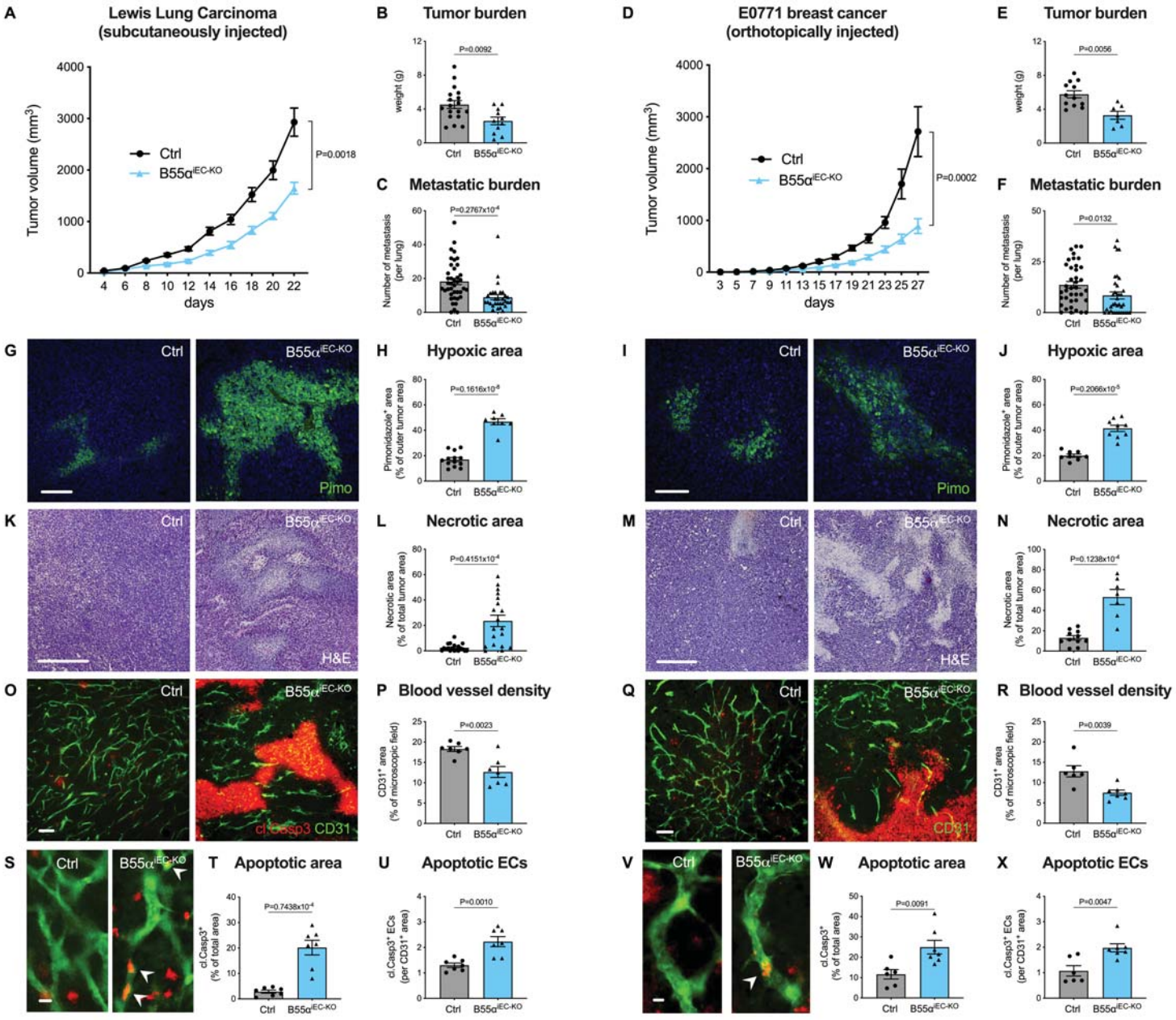
A
Lewis Lung Carcinoma
(subcutaneously injected)
Tumor volume (mm3)
Ctrl
B55αiEC-KO
P=0.0018
days
B
Tumor burden
weight (g)
P=0.0092
C
Metastatic burden
Number of metastasis (per lung)
P=0.2767x10-4
D
E0771 breast cancer
(orthotopically injected)
P=0.0002
E
Tumor burden
P=0.0056
F
Metastatic burden
P=0.0132
G
Pimo
H
Hypoxic area
Pimonidazole+ area (% of outer tumor area)
P=0.1616x10-6
I
J
Hypoxic area
P=0.2066x10-5
K
H&E
L
Necrotic area
Necrotic area (% of total tumor area)
P=0.4151x10-4
M
N
Necrotic area
P=0.1238x10-4
O
cl.Casp3 CD31
P
Blood vessel density
CD31+ area (% of microscopic field)
P=0.0023
Q
CD31
R
Blood vessel density
P=0.0039
S
T
Apoptotic area
cl.Casp3+ (% of total area)
P=0.7438x10-4
U
Apoptotic ECs
cl.Casp3+ ECs (per CD31+ area)
P=0.0010
V
W
Apoptotic area
P=0.0091
X
Apoptotic ECs
P=0.0047

Figure 4

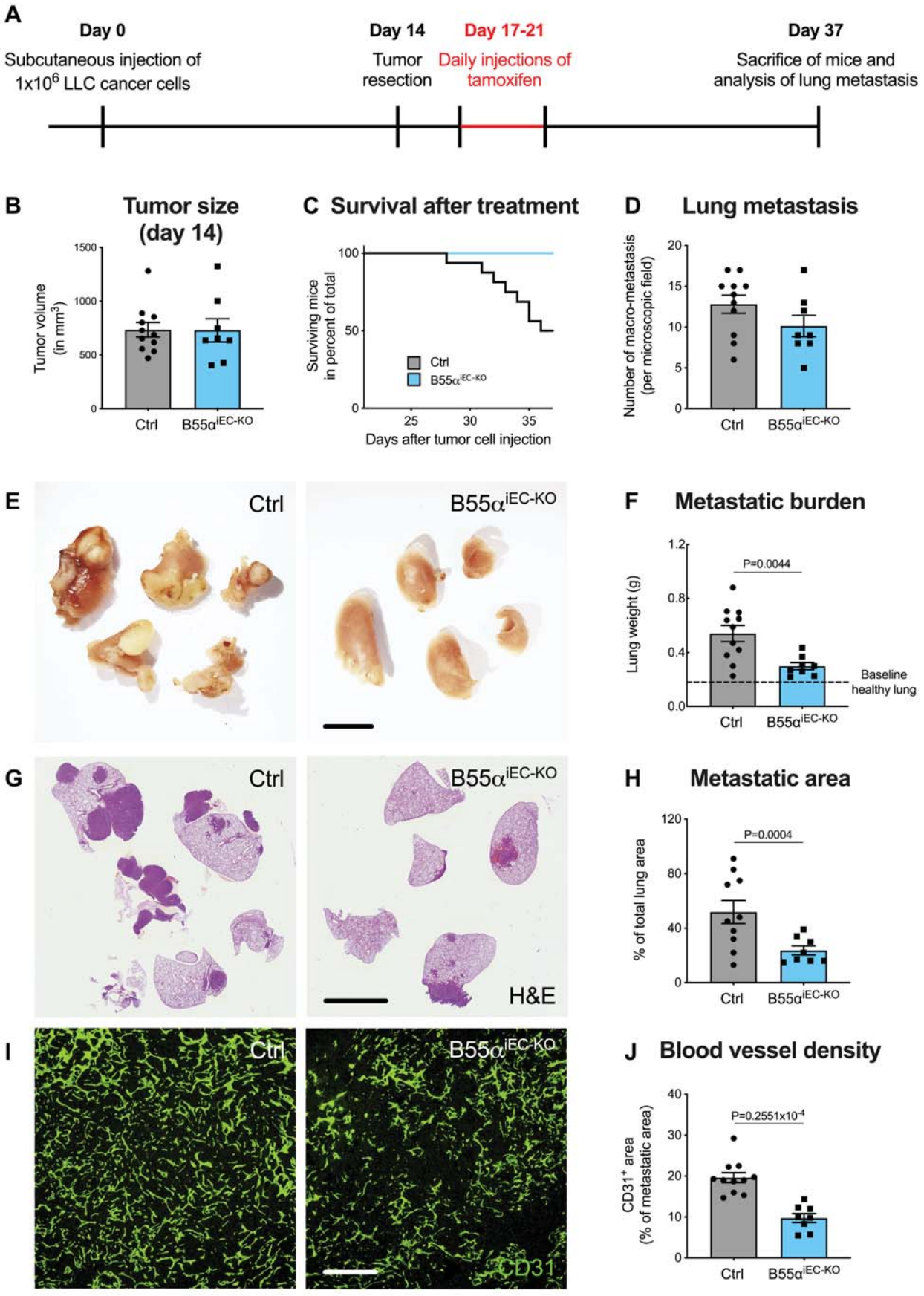
A
Day 0
Subcutaneous injection of 1x10^6 LLC cancer cells
Day 14
Tumor resection
Day 17-21
Daily injections of tamoxifen
Day 37
Sacrifice of mice and analysis of lung metastasis
B
Tumor size (day 14)
Tumor volume (in mm3)
1500
1000
500
0
Ctrl
B55α iEC-KO
C Survival after treatment
Surviving mice in percent of total
100
50
0
Ctrl
B55α iEC-KO
25
30
35
Days after tumor cell injection
D Lung metastasis
Number of macro-metastasis (per microscopic field)
20
15
10
5
0
Ctrl
B55α iEC-KO
E
Ctrl
B55α iEC-KO
F Metastatic burden
Lung weight (g)
1.2
0.8
0.4
0.0
P=0.0044
Baseline healthy lung
Ctrl
B55α iEC-KO
G
Ctrl
B55α iEC-KO
H&E
H Metastatic area
% of total lung area
120
80
40
0
P=0.0004
Ctrl
B55α iEC-KO
I
Ctrl
B55α iEC-KO
CD31
J Blood vessel density
CD31+ area (% of metastatic area)
40
30
20
10
0
P=0.2551x10-4
Ctrl
B55α iEC-KO

Figure 5

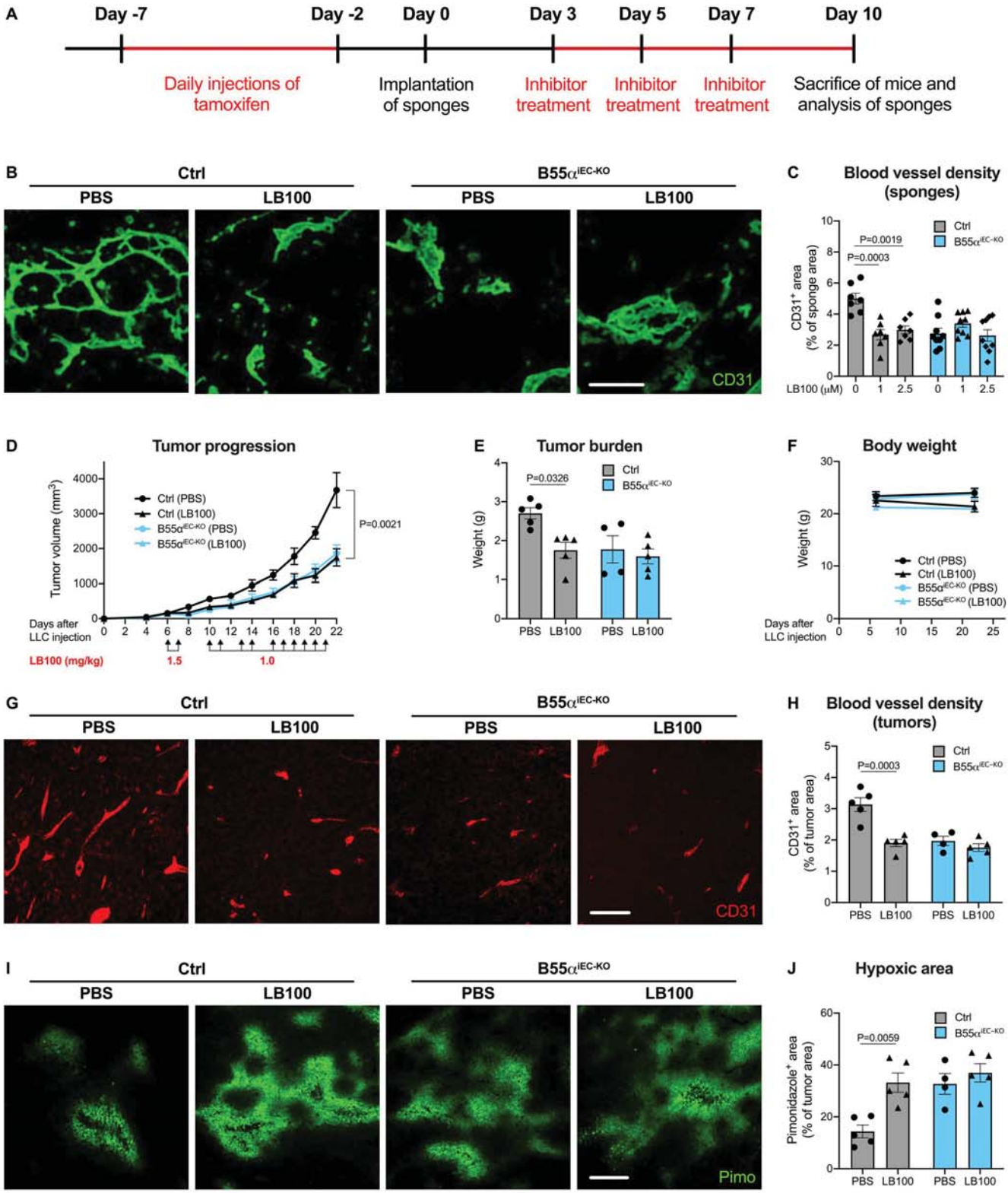
A
Day -7
Day -2
Day 0
Day 3
Day 5
Day 7
Day 10
Daily injections of tamoxifen
Implantation of sponges
Inhibitor treatment
Inhibitor treatment
Inhibitor treatment
Sacrifice of mice and analysis of sponges
B
Ctrl
B55α^IEC-KO
PBS
LB100
PBS
LB100
CD31
C
Blood vessel density (sponges)
CD31+ area (% of sponge area)
P=0.0019
P=0.0003
Ctrl
B55α^IEC-KO
LB100 (μM) 0 1 2.5 0 1 2.5
D
Tumor progression
Tumor volume (mm3)
Ctrl (PBS)
Ctrl (LB100)
B55α^IEC-KO (PBS)
B55α^IEC-KO (LB100)
P=0.0021
Days after LLC injection
LB100 (mg/kg)
1.5
1.0
E
Tumor burden
Weight (g)
P=0.0326
Ctrl
B55α^IEC-KO
PBS LB100 PBS LB100
F
Body weight
Weight (g)
Ctrl (PBS)
Ctrl (LB100)
B55α^IEC-KO (PBS)
B55α^IEC-KO (LB100)
Days after LLC injection
G
Ctrl
B55α^IEC-KO
PBS
LB100
PBS
LB100
CD31
H
Blood vessel density (tumors)
CD31+ area (% of tumor area)
P=0.0003
Ctrl
B55α^IEC-KO
PBS LB100 PBS LB100
I
Ctrl
B55α^IEC-KO
PBS
LB100
PBS
LB100
Pimo
J
Hypoxic area
Pimonidazole+ area (% of tumor area)
P=0.0059
Ctrl
B55α^IEC-KO
PBS LB100 PBS LB100

Figure 6

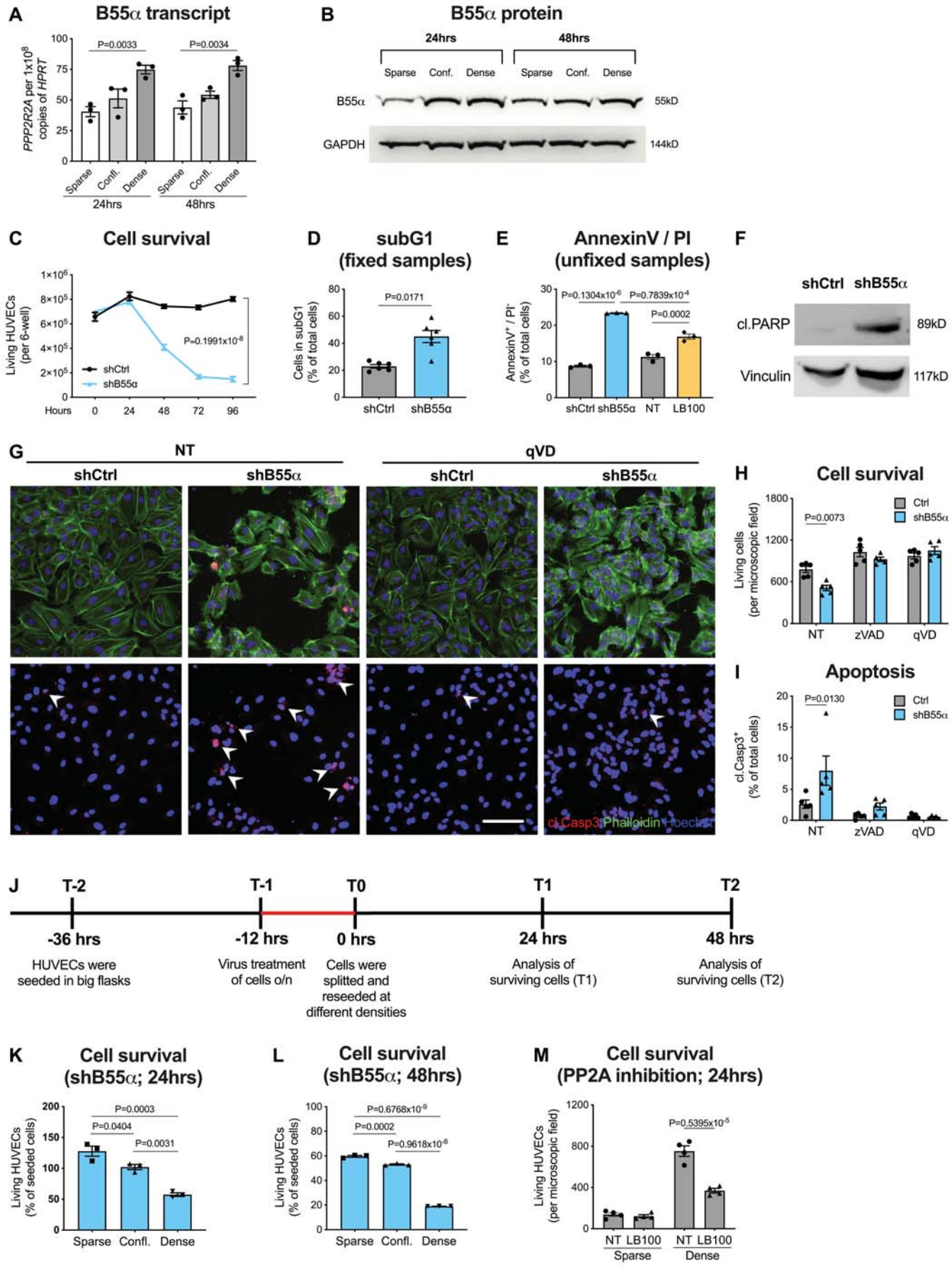
A
B55α transcript
PPP2R2A per 1x10^8 copies of HPRT
P=0.0033
P=0.0034
Sparse
Confl.
Dense
24hrs
48hrs
B
B55α protein
24hrs
48hrs
Sparse
Conf.
Dense
B55α
55kD
GAPDH
144kD
C
Cell survival
Living HUVECs (per 6-well)
P=0.1991x10^-8
shCtrl
shB55α
Hours
D
subG1 (fixed samples)
Cells in subG1 (% of total cells)
P=0.0171
E
AnnexinV / PI (unfixed samples)
AnnexinV+ / PI- (% of total cells)
P=0.1304x10^-6
P=0.7839x10^-4
P=0.0002
NT
LB100
F
shCtrl
shB55α
cl.PARP
89kD
Vinculin
117kD
G
NT
qVD
shCtrl
shB55α
cl.Casp3 Phalloidin Hoechst
H
Cell survival
Living cells (per microscopic field)
P=0.0073
Ctrl
shB55α
NT
zVAD
qVD
I
Apoptosis
cl.Casp3+ (% of total cells)
P=0.0130
J
T-2
T-1
T0
T1
T2
-36 hrs
HUVECs were seeded in big flasks
-12 hrs
Virus treatment of cells o/n
0 hrs
Cells were splitted and reseeded at different densities
24 hrs
Analysis of surviving cells (T1)
48 hrs
Analysis of surviving cells (T2)
K
Cell survival (shB55α; 24hrs)
Living HUVECs (% of seeded cells)
P=0.0003
P=0.0404
P=0.0031
L
Cell survival (shB55α; 48hrs)
P=0.6768x10^-9
P=0.0002
P=0.9618x10^-8
M
Cell survival (PP2A inhibition; 24hrs)
P=0.5395x10^-5

Figure 7

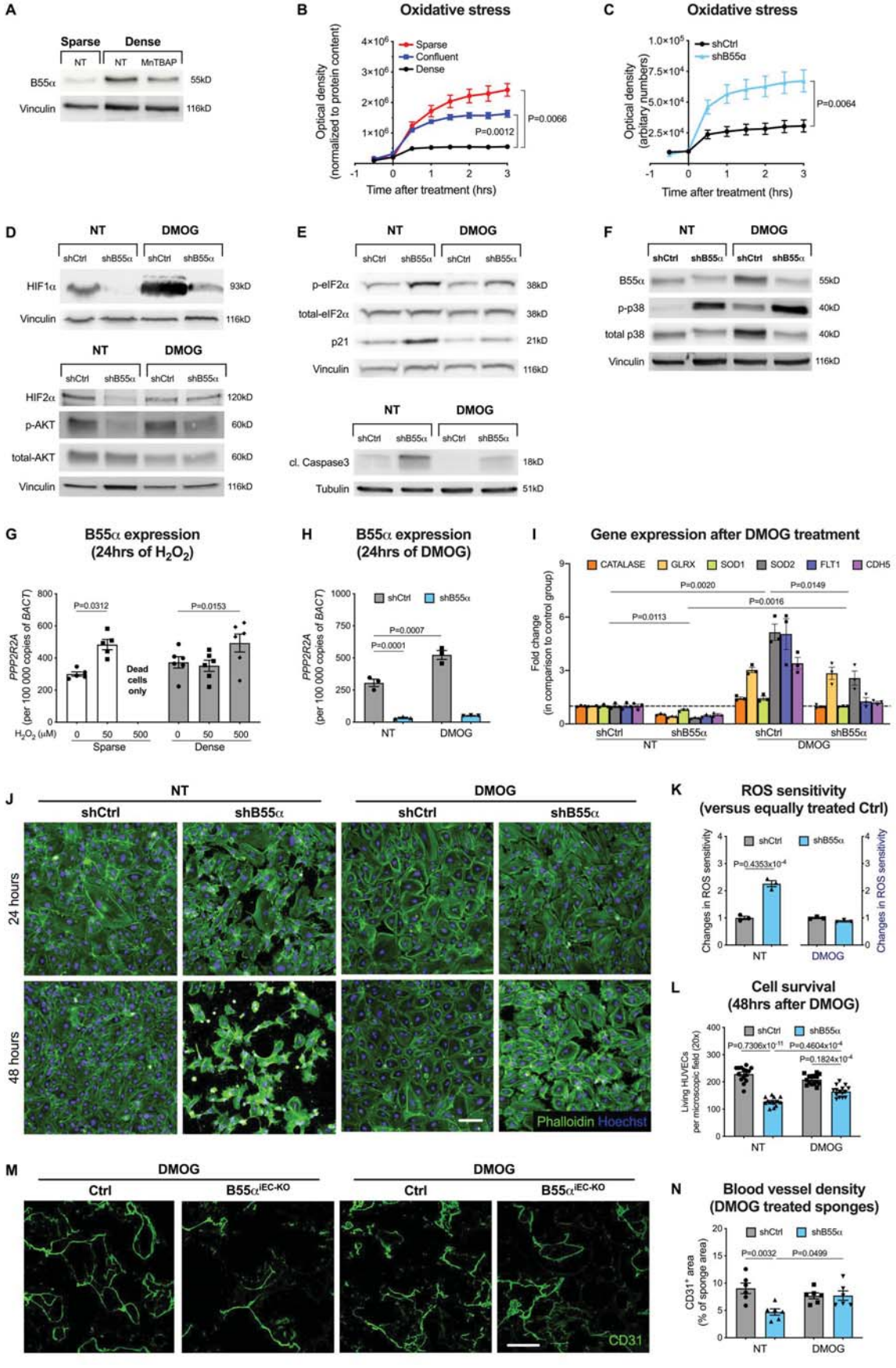
A
Sparse
Dense
NT
NT
MnTBAP
B55α
55kD
Vinculin
116kD
B
Oxidative stress
Optical density (normalized to protein content)
Sparse
Confluent
Dense
P=0.0066
P=0.0012
Time after treatment (hrs)
C
Oxidative stress
Optical density (arbitary numbers)
shCtrl
shB55α
P=0.0064
Time after treatment (hrs)
D
NT
DMOG
shCtrl
shB55α
HIF1α
93kD
Vinculin
116kD
HIF2α
120kD
p-AKT
60kD
total-AKT
60kD
E
p-eIF2α
38kD
total-eIF2α
38kD
p21
21kD
cl. Caspase3
18kD
Tubulin
51kD
F
B55α
55kD
p-p38
40kD
total p38
40kD
G
B55α expression (24hrs of H2O2)
PPP2R2A (per 100 000 copies of BACT)
P=0.0312
P=0.0153
Dead cells only
H2O2 (μM)
Sparse
Dense
H
B55α expression (24hrs of DMOG)
P=0.0007
P=0.0001
I
Gene expression after DMOG treatment
CATALASE
GLRX
SOD1
SOD2
FLT1
CDH5
Fold change (in comparison to control group)
P=0.0020
P=0.0149
P=0.0016
P=0.0113
J
24 hours
48 hours
Phalloidin Hoechst
K
ROS sensitivity (versus equally treated Ctrl)
Changes in ROS sensitivity
P=0.4353x10-4
L
Cell survival (48hrs after DMOG)
Living HUVECs per microscopic field (20x)
P=0.7306x10-11
P=0.4604x10-4
P=0.1824x10-4
M
Ctrl
B55αiEC-KO
CD31
N
Blood vessel density (DMOG treated sponges)
CD31+ area (% of sponge area)
P=0.0032
P=0.0499

Figure 8

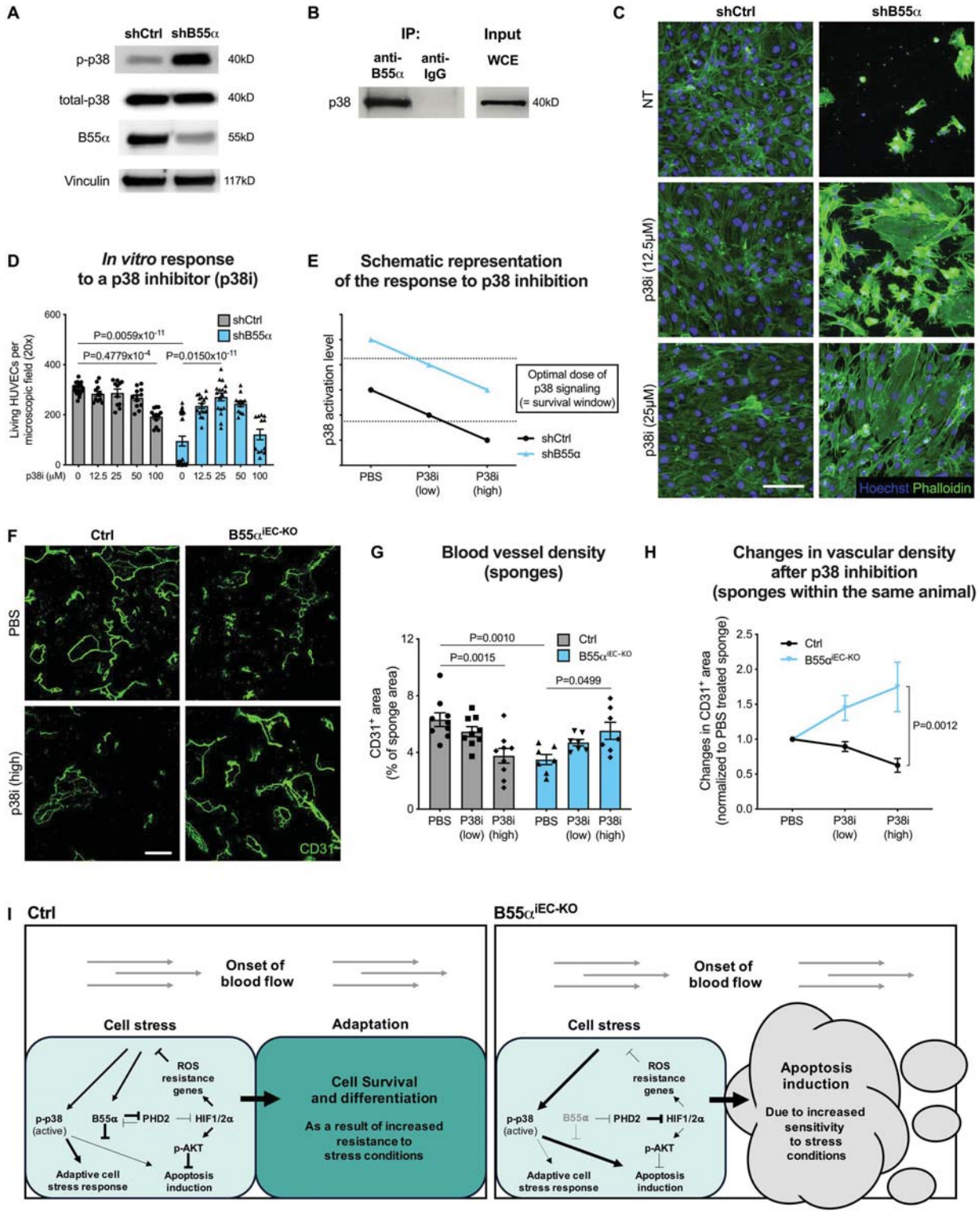
A
shCtrl shB55α
p-p38 40kD
total-p38 40kD
B55α 55kD
Vinculin 117kD
B
IP:
anti-B55α anti-IgG
Input WCE
p38 40kD
C
shCtrl shB55α
NT
p38i (12.5μM)
p38i (25μM)
Hoechst Phalloidin
D
In vitro response to a p38 inhibitor (p38i)
Living HUVECs per microscopic field (20x)
shCtrl shB55α
P=0.0059x10-11
P=0.4779x10-4
P=0.0150x10-11
p38i (μM) 0 12.5 25 50 100 0 12.5 25 50 100
E
Schematic representation of the response to p38 inhibition
p38 activation level
Optimal dose of p38 signaling (= survival window)
shCtrl
shB55α
PBS P38i (low) P38i (high)
F
Ctrl B55α iEC-KO
PBS
p38i (high)
CD31
G
Blood vessel density (sponges)
CD31+ area (% of sponge area)
P=0.0010
P=0.0015
P=0.0499
Ctrl
B55α iEC-KO
PBS P38i (low) P38i (high) PBS P38i (low) P38i (high)
H
Changes in vascular density after p38 inhibition (sponges within the same animal)
Changes in CD31+ area (normalized to PBS treated sponge)
Ctrl
B55α iEC-KO
P=0.0012
PBS P38i (low) P38i (high)
I
Ctrl
B55α iEC-KO
Onset of blood flow
Cell stress
Adaptation
ROS resistance genes
p-p38 (active)
B55α
PHD2
HIF1/2α
p-AKT
Adaptive cell stress response
Apoptosis induction
Cell Survival and differentiation
As a result of increased resistance to stress conditions
Apoptosis induction
Due to increased sensitivity to stress conditions